Supplement to Lecture 8
More about surface plasmons

Some historical background

Very recent news articles (April 2011)

Surface plasmon lasers, modulators, and LEDs

Weird Light & Plasmons 2

Last time, I talked about how weird light really is, and how it is simultaneously made up of waves, and of particles called photons. Trunk lines of glass fibre are being laid across the world, and inside these optic fibres, beams of light are shifting huge amounts of data. So we are gradually shifting from "electrons" and "electronics", to "photons" and "photonics". But when you get down to the size of the wavelength of light, you enter the land of Quantum Mechanics, where everything is really weird.

Back in 1989, Thomas Ebbesen from the NEC Research Institute in Princeton, New Jersey, was playing with a special sheet of gold foil. It had some 100 million tiny holes in it, each about 300 nanometres (nm) across. A nanometer is really small - one billionth of a metre, or a millionth of a millimeter. Now 400 nm is roughly the wavelength of blue light, and it's the smallest wavelength that our eyes can see. Green light is in the middle of the rainbow at around 525 nm, and red light is at the top end of what our eyes can see with a wavelength of about 700 nm.

So these 100 million holes (each 300 nm across) were all smaller than the shortest wavelength of visible light (which is blue light at 400 nm). It's like trying to stuff a basketball into a hole the size of tennis ball - it just won't go. There is a well-accepted Quantum Theory of optics which tells us that actually about one thousandth of the light that falls on the holes should somehow sneak through. But forget the theory.

Back in 1989, Thomas Ebbesen measured that well over 100% of the light that was hitting the holes on one side, was getting through the holes to the other side, and out. There was more light coming out of the holes than was going into them! It was as though the metal between the holes was gathering the light and magically funneling the light to the holes. Ebbesen did his experiments many more times, in many different ways, and still there was more light getting through the holes than was landing on them. Nobody could explain these weird results, so he didn't even write about them in a science magazine.

This all changed in 1998, when Peter Wolff, a theoretical physicist, joined NEC and found out about these weird holes that funneled light. Now Wolff had a special interest in how electrons behaved on the surface of a metal. He already knew that electrons ripple around on the surface in strange waves called " surface plasmons". If you want to get technical, the physicists say that these strange waves are "collective electronic excitations, or charge density waves, which are characterized by intense electromagnetic fields confined to the surface". In plain English, the electrons behave like waves, not particles, and these waves ripple around on the surface of metals - a bit like how waves ripple on the surface of the water of a pond when small boats sail across it.

By an amazing coincidence for Ebbesen back in 1989, there was an accidental close match between the incoming light and the plasmons. By a lucky coincidence, the incoming light and the plasmons each had the same energy and momentum. So the incoming light was being absorbed by these strange waves on the surface of the gold (these surface plasmons) and then the surface plasmons were traveling through the holes to the other side, and when they got to the other side of the metal foil, they were collapsing and emitting the light.

That's really weird.

But then it got weirder.

The next experiment just had one single small hole. The metal foil was engraved on each side with a whole set of concentric rings, like a bullseye. These rings didn't go all the way through the metal, they were just grooved into the foil. Again, the light landing on the metal got absorbed by the surface plasmon waves, which went through the single hole and emitted the light on the other side - but only from the hole.

So why would these scientists have been spending their time on poking light through a hole?

One use would be to groove incredibly thin lines in computer chips - making them faster. Or, you could use the Bullseye Effect to focus and send light exactly where you wanted to.

Or how about a medical use? Shine light onto chemicals that are stuck to a metal surface, and the plasmons could slowly deliver drugs over days, and weeks.
These plasmons could put us light years ahead of where we stand today…

Tag-team entanglement

In quantum mechanics, when two particles cannot be described meaningfully by two separate wavefunctions they are said to be entangled. As a result, any manipulation or measurement of one of the pair has an immediate effect on the state of the other, regardless of the distance between them. This counterintuitive effect — famously dismissed by Einstein as requiring implausible "spooky actions at a distance" — is at the heart of research into quantum computing and quantum cryptography.

Entanglement is relatively fragile — environmental decoherence effects can readily split the single wavefunction of an entangled system into two or more distinct, non-entangled, particle wavefunctions. This fragility usually places constraints on the way in which such systems can be handled. But in this week's Nature, Erwin Altewischer and colleagues demonstrate the transmission of entanglement between systems of entirely different particles, without any catastrophic decoherence.

Photons are usually used in entanglement experiments for three simple reasons. Entangled pairs of photons are readily produced — for example by the spontaneous splitting of a single photon in a nonlinear crystal — they are easy to transmit over long distances, and their entanglement can be verified statistically. Altewischer and co-workers used entangled photons for another reason: they readily interact with other types of particles — in this case, surface plasmons.

Surface plasmons are quasiparticles formed from collective excitations of conduction electrons at the surface of a metal or semiconductor. The wave-like nature of surface plasmons has been understood for some time, but their quantum nature has never been explicitly verified. Recent studies have shown that by forming a periodic array of pinholes in a metallic thin film, the dispersion relation for surface plasmons in the film can be altered to enhance their resonant coupling with light. Such coupling results in a surface-plasmon-mediated enhancement of light transmission through these films.

By placing identically formed hole arrays in the paths of two entangled photon beams, Altewischer et al. tested whether the surface plasmons preserve the entanglement during light transmission. The answer they got was a resounding yes. In the absence of hole arrays, the visibility of the biphoton interference fringe — a measure of the degree of entanglement between the beams — was 97.0–99.3%. Placing both arrays into both beams caused almost no change in their entanglement, resulting in visibilities of around 97.1%. Similar results were found using only one array in one of the beams.

These results suggest that entanglement is perhaps more robust than expected. But more significantly, it shows for the first time the essential quantum nature of surface plasmons — involving the collective motion of some 1010 electrons — a vivid demonstration of the occurrence of quantum phenomena at macroscopic scales.

Plasmon-assisted transmission of entangled photons

E. ALTEWISCHER, M. P. VAN EXTER & J. P. WOERDMAN

The state of a two-particle system is said to be entangled when its quantum-mechanical wavefunction cannot be factorized into two single-particle wavefunctions. This leads to one of the strongest counter-intuitive features of quantum mechanics, namely non-locality. Experimental realization of quantum entanglement is relatively easy for photons; a starting photon can spontaneously split into a pair of entangled photons inside a nonlinear crystal. Here we investigate the effects of nanostructured metal optical elements on the properties of entangled photons. To this end, we place optically thick metal films perforated with a periodic array of subwavelength holes in the paths of the two entangled photons. Such arrays convert photons into surface-plasmon waves-optically excited compressive charge density waves-which tunnel through the holes before reradiating as photons at the far side. We address the question of whether the entanglement survives such a conversion process. Our coincidence counting measurements show that it does, so demonstrating that the surface plasmons have a true quantum nature. Focusing one of the photon beams on its array reduces the quality of the entanglement. The propagation of the surface plasmons makes the array effectively act as a 'which way' detector.
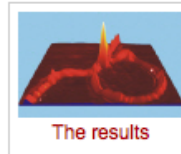
Surface plasmons squeeze light

The backbone of the world's communication system is a network of optical fibres that carry information in the form of light pulses. Large volumes of data can be transmitted very efficiently down these fibres but bottlenecks in the system occur when the light pulses are converted into electrical signals at various "junction boxes" that ensure information reaches its correct destination. The telecommunications industry, among others, is therefore extremely interested in microphotonic circuits that can manipulate light pulses directly and therefore increase data rates.

Physicists in Denmark and France led by Sergey Bozhevolnyi of the University of Aalborg have developed a new class of waveguide that could get round one of the biggest obstacles to photonic circuits. The devices allow light at telecommunications wavelengths to be "squeezed" to below the diffraction limit, allowing it to pass though small regions such as channels on a chip without being significantly lost (*Nature* **440** 508).

Diffraction means that only a tiny amount of light can pass through a hole that is narrower than the wavelength of the light, and the light that *is* transmitted emerges in all directions. This can be problematic, for example, in optical lithography where diffraction prevents the fabrication of semiconductor features below a certain size. In telecommunications, where the light typically has a wavelength of 1.5 microns, light cannot pass though the channels used to guide electrons in today's silicon chips because they are too small.

The results

One way to overcome this problem is to use light waves to excite the collective wavelike motions of billions of electrons on the surface of metals. Unlike the light waves themselves, these "surface plasmons" are not restricted by the diffraction limit of light. Indeed, Bozhevolnyi and co-workers previously showed that the plasmons can be used to guide light through grooves in gold that are much narrower than the wavelength of the light used.

Discussing channel plasmon-polaritons

Now, the Denmark-France team has taken this work a step further by using a new class of surface plasmons called channel plasmon-polaritons -- electromagnetic waves that originate at the interface of a metal and an insulating dielectric such as air. The researchers have shown that these plasmons can guide and manipulate light along the bottom of sub-wavelength V-shaped grooves in a gold film without significant propagation losses (see figure). This is because the surface plasmons remain tightly bound to the interface and thus concentrate the light into a volume that is less than one wavelength across.

Channel plasmon-polaritons can be used to transmit light signals for wavelengths of around 1.5 microns -- just right for telecommunications applications. Furthermore, the propagation length of a plasmon at a planar gold-air interface is around 1mm, which is long enough to optically connect two devices on a chip.

"Our technique is so good that it can already be used for many practical applications, such as ultracompact optical interconnects, interferometers and waveguide-ring resonators," explains Bozhevolnyi. "It should also be borne in mind that the channel plasmon-polaritons are bound to and propagate along the metal surface, thereby allowing for natural integration with electrical circuits."

Physics and Technology Forefronts

Catching an electron wave with emerging plasmon applications.

By Jennifer Ouellette

When light strikes a metallic surface, it generates electron waves, called plasmons. This remarkable effect was discovered in 1897 by Robert W. Wood, a physics professor at Johns Hopkins University . Wood was also the first person to unwittingly record the energy lost as heat by plasmons skimming along the surface of metals in 1902.

It took 40 years for Italian physicist Ugo Fano to provide an explanation: metals are not perfect conductors. A conducting surface can guide light as a 2D surface wave plasmons are also known as two-dimensional light–and those waves absorb energy. Hence, Wood's anomalous observations of energy loss in the light reflected from metallic surfaces. Their unusual properties make surface plasmons extremely promising for a wide range of applications, including plasmon microscopes and "super-lenses," plasmon-based nanoparticle biosensors, and electronic circuits capable of operating at optical frequencies.

'Nanorice' shown in the images above, can be used to map the surfaces of biological cells.

A "plasmon microscope" formed with a glycerin drop (left) creates an image of a 30 μm x 30 μm array of "nanoholes" (blue square), in which the triplets of the 100 nm diameter holes can be resolved (right).

Cutting-Edge Microscopes . Plasmons can enable scientists to see fine details that were previously undetectable. For instance, a team of scientists at the University of Maryland led by Igor Smolyaninov, along with colleagues at Queen's University in Belfast, Ireland, are developing a two-dimensional plasmon microscope, ideal for imaging living cells, that could operate much like a point-and-shoot camera and reveal much more detail that currently available with existing imaging techniques. They were able to image tiny objects with spatial resolutions of 60 nm, further reduced to 30 nm with a bit of mathematical tweaking. The UMD team believes they can improve the resolution even further, down to around 10 nm.

A sample is placed on a metal-coated glass surface and covered with a drop of glycerin. Laser light shines through the glass and produces surface plasmons in the metal. The glycerin acts like a parabolic dish that can collect plasmons sprayed out from the sample at its focal point. It then forms them into something like a "plasmon beam" that goes back down towards the metal surface. Part of that beam bounces back up and can be seen with a regular light microscope. The performance is close to what an electron microscope might achieve, but involves no vacuum, high voltage or elaborate specimen preparation.

Other planned improvements include replacing the micromanipulators currently used to adjust the glycerin droplet's shape by hand with solid mirrors etched on the glass using lithography — an important step towards building a practical device. This would enable scientists to buy these special glass slides to use with any microscope: any lab could achieve electron microscopy resolution for the cost of a regular microscope. Nor would there be a need for special sample preparation. Movies might even be possible, since the image is taken all at once, rather than one pixel at a time. State-of-the-art lithography cannot yet produce sufficiently smooth mirrors to match that of the glycerin drop's surface, but the UMD researchers are hopeful that the technology will continue to improve rapidly to make it possible in the near future.

Super-Lensing . Other researchers are exploiting plasmons to create "super lenses," relying on tiny nanoparticles to amplify and focus the light shining on a given sample. Scientists at the University of Texas, for example, have built a "super lens" and used it in a device to take pictures just below the surface of thin material substrates. According to Gennady Shvets, by combining his "super lens" with near-field scanning optical microscopy, he was able to achieve microscope resolutions as good as 1/20th of a wavelength in the mid-infrared range of light.

This in turn enabled him to observe "giant transmission," in which light falls on a surface covered with holes much smaller than the wavelength of the light. Even though the total area of the holes comprised a mere 6% of the total surface area, 30% of the light nonetheless came through, thanks to the presence of plasmons. It is very difficult to image objects smaller than half the wavelength of the light being used for the imaging, but Shvets and his colleagues were able to achieve much higher resolution because there was less diffraction.

Meanwhile, at Rice University, researchers have created rice-shaped particles of gold and iron oxide, called "nanorice"–so named because when magnified the structures resemble tiny grains of rice that they hope to attach to the probe tips of scanning microscopes to map out the surfaces of biological cells. According to group leader Naomi Halas, nanorice is similar to an earlier structure she invented in 1998 called nanoshells. Both are made of a non-conducting core covered by a metallic shell. Changing the shape of a metal at the nanoscale enables researchers to modify the properties of the plasmon waves produced. Spheres and rods are the most optically useful shapes, and nanorice combines the best properties of both.

Nanoshells and nanorice can also serve as "super-lenses," amplifying light waves and focusing them to spots far smaller than a wavelength light. In fact, Halas reports that nanoshells are about 10,000 times more effective at surface-enhanced Raman spectroscopy (SERS) than traditional methods. Raman scattering is routinely used by medical researchers, drug designers, and chemists to determine the precise chemical makeup of materials. So single grains of nanorice could provide the needed field intensities to characterize biomolecules like proteins and DNA that adsorb on a particle. They could also be used not just to identify, but eradicate cancer cells in rats.

Integrated "Plasmonics." To date, it's proven difficult to combine photonic components — such as fiber optic cables — with electronic components like wires and transistors because of their mismatched capabilities and size scales. Photonic components can carry a lot of data — witness the explosion in broadband data transmission rates — but are bulkier than electronic components, which in turn can carry less data. Ideally scientists would like to be able to combine the best features of both onto a single chip in an emerging new discipline known as plasmonics.
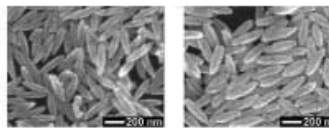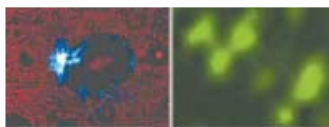
Plasmons might be the key to achieving true integration on a single chip, since they operate at optical frequencies — typically 100,000 times greater than the frequency of even the most cutting-edge microprocessors — and the higher the frequency of the wave, the more information you can transport over it. Yet they take up much less space because their wavelengths are much smaller than the light used to create them. In such devices, light would be converted into plasmons, which propagate along a metallic surface with a wavelength smaller than the original light. The plasmons could then be processed with their own 2D optical components– mirrors, waveguides, or lenses–and then later converted back into light, or into electrical signals.

Nader Engheta of the University of Pennsylvania believes that nanoparticles–including those capable of supporting plasmon excitations–could be configured to act as nanometer-scale capacitors, resistors and inductors: the basis elements of an electrical circuit. But in this case, the circuit would operate not at radio or microwave frequencies, but at optical frequencies. This would enable the further miniaturization (down to about 30-50 nm) of optical components and the direct processing of optical signals with nano-antennas, nano-circuit filters, nano-waveguides, and nano-resonators. It could even lead to possible applications in nano-computing, nano-data storage, molecular signaling and molecular-optical interfacing.

Physicists in Denmark and France led by Sergey Bozhevolnyi of the University of Aalborg have developed a waveguide that could allow light at fiber-optic wavelengths to be "squeezed" to below the diffraction limit, allowing it to pass though small regions such as channels on a chip without being significantly lost.

Bozhevolnyi's team used a new class of surface plasmons called channel plasmon-polaritons — electromagnetic waves that originate at the interface of a metal and an insulating dielectric such as air. These plasmons can guide and manipulate light along the bottom of V-shaped grooves in a gold film without significant propagation losses. This is because the surface plasmons remain tightly bound to the interface and thus concentrate the light into a volume that is less than one wavelength across.

Channel plasmon-polaritons can be used to transmit light signals for wavelengths of around 1.5 microns — just right for telecommunications applications. Furthermore, the propagation length of a plasmon at a planar gold-air interface is around 1 mm, which is long enough to optically connect two devices on a chip.

Cloak and Dagger. In 2005, scientists at the University of Pennsylvania announced that they could potentially use plasmon coatings as a cloaking device to render objects invisible by creating a kind of "shell" around the object. Plasmon waves limit light scattering off an object because they resonate at the same frequency as the light striking them, so they cancel each other out. This makes the object in question very difficult to detect.

The roots of their research date back to 1998, when researchers led by Thomas Ebbesen of the Louis Pasteur University in Strasbourg, France shone light on a sheet of gold foil that contained millions of tiny holes. The holes were smaller than the wavelength of the light, and Ebbesen expected no light to get through. Instead, more light came out the other side than what hit the holes. Follow-up research found that plasmons were snagging light and stuffing it through the holes. When the energy and momentum of the photons match the energy and momentum of the plasmons, the photons are absorbed and radiated again on the other side.

Practically speaking, the technology, if developed, might be used in antiglare materials or to improve microscopic imaging. A more futuristic goal is that an entire aircraft might be made transparent to radio waves or some other long-wavelength detector.

But cloaking ability would depend on an object's size, so that only with very small things — items that are already microscopic or nearly so — could the visible light be rendered null. A human could be made impossible to detect in longer-wavelength radiation such as microwaves, but not in visible light.

Anything not perfectly ball-shaped presents additional problems. The researchers' calculations suggest "homogeneous spherical objects" in the nanoscale range could be rendered optically invisible.

More than 100 years after their serendipitous discovery, an increasing number of researchers are catching an electron wave. As a result surface plasmons are emerging as a critical element in many next-generation technological applications because of the remarkable properties. Further research and development is needed before such applications become truly enabled, but the future of plasmons appears as bright as a shiny metallic mirror.

Nanotechnology

Plasmonic waveguides based on synthetic nanomembranes

Zoran Jakšić
Optics and electronics are merged on the nanoscale to facilitate introduction of biomimetic principles in nano-optics.
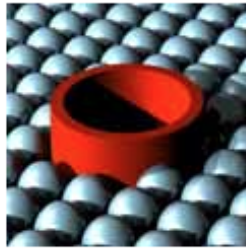
Structuring metal dielectrics with nanometer-scale precision enables electromagnetic-field concentration and control at the subwavelength level. Use of surface-plasmon polaritons (SPPs), evanescent waves propagating at a conductor-dielectric interface, has ushered in the field of plasmonics.[1,2] Plasmonic waveguides and circuits will be critical to a new generation of devices with the compact dimensions of integrated electronics and the speed of photonics.[3] Existing applications of plasmonics include ultrasensitive chemical and biological sensors,[4] plasmon nanoguides and circuits,[5] and photovoltaic cells.[6] Photonics is vastly extended by plasmonic nanostructures, including subwavelength plasmonic crystals[7] and plasmonic metamaterials.[8]

The primary limitations of plasmonic materials are heavy absorption losses, large frequency dispersions, and a limited choice of materials.[9] Longer propagation paths and larger design freedom could be ensured through use of synthetic free-standing nanomembranes, quasi-2D structures with extremely large aspect ratios.[10] Such structures are intrinsically symmetric in an electromagnetic sense, ensure much lower losses, and therefore support long-range SPP propagation[11–13] (see Figure 1). In contrast to conventional SPP guides with bulk substrates, here SPPs propagate along a quasi-2D guide. A nanomembrane is less than 100nm thick, with lateral dimensions often larger than 1cm. In spite of their enormous aspect ratios, nanomembranes are quite robust and even allow manipulation with free hands.[14,15] They are probably the only element from the nanotechnology toolbox that can be seen with an unaided eye and manipulated without special equipment.
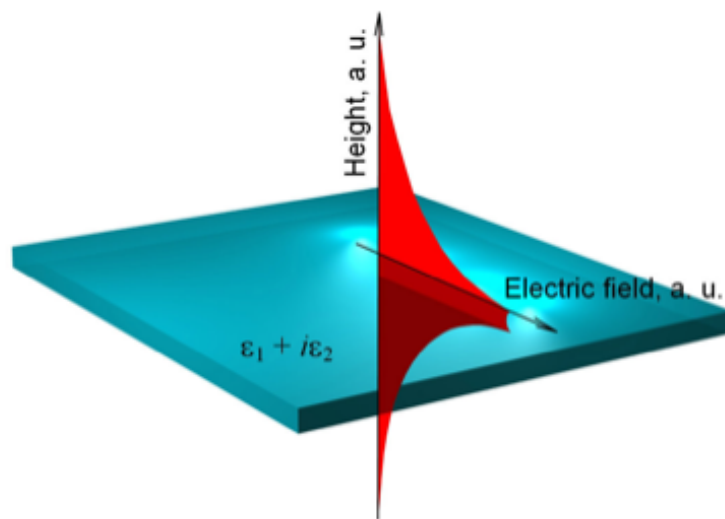

Figure 1. *Long-range surface-plasmon-polariton (SPP) propagation on a self-supported nanomembrane. ε_1, ε_2: Dielectric functions. a.u.: Arbitrary units.*

In our research, we choose to produce plasmonic nanomembrane guides through multifunctionalization.[16] A biological nanomembrane without functionalization would be a simple inanimate object. Synthetic-nanomembrane nanofunctionalization vastly expands their applicability. Primary approaches to membrane multifunctionalization include using nanofillers, lamination (multilayering), additive and subtractive patterning, and surface sculpting (see Figure 2).
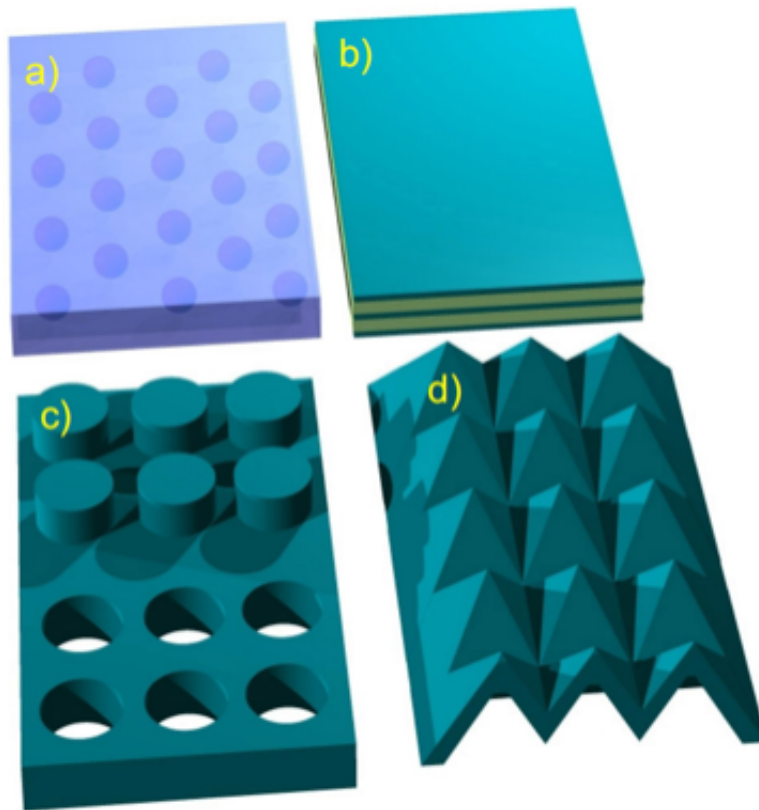
Figure 2).

Figure 2. *Nanomembrane multifunctionalization. (a) Nanofillers, (b) lamination, (c) additive (top) and subtractive (bottom) patterning, and (d) surface sculpting.*

One may incorporate nanofillers into nanomembranes. Examples include plasmonic metal-nanoparticle arrays,[17] which themselves may serve as plasmonic guides, but also other components such as carbon nanotubes, which also mechanically reinforce nanomembranes. Another approach is to laminate a larger number of strata, thereby obtaining multilayer plasmonic crystals.[18] Methods for this approach include the layer-by-layer technique,[19] Langmuir-Blodgett deposition, and dip-and-drop coating.[16] Patterning by rendering protrusions or apertures can be effected, for example, by directed energy or particle beams.[20] This enables fabrication of complex structures, such as fishnet-type negative-refractive-index metamaterials. Nanomembrane waveguides can also be sculpted to form various 3D shapes[21,22] (see Figure 3). Obviously, two or more of these may be combined.
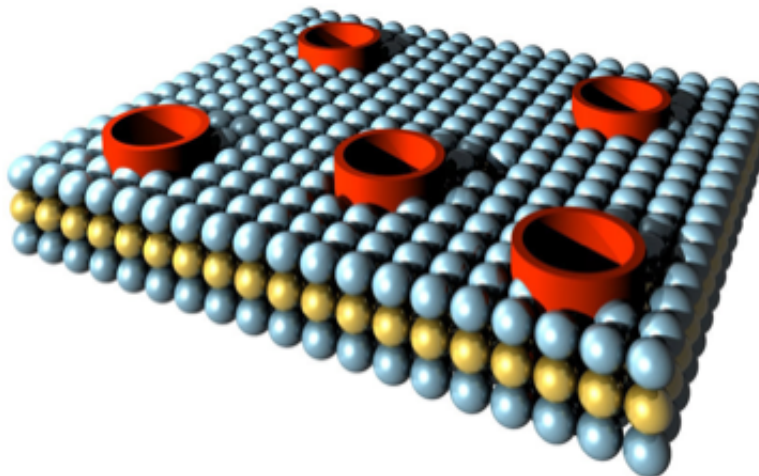

Figure 3. *Artificial ion channels (red cylinders) built into a three-layer nanomembrane.*

One of our research directions is lamination of nanomembranes with layers of transparent conductive oxides.[23] These materials are seen as a viable low-loss alternative to metals in plasmonics.[9] We used indium oxide, indium-doped tin oxide, and aluminum-doped zinc oxide nanoparticles synthesized from nonaqueous solution and deposited them using dip-or-drop coating.[23]

Another research direction is aimed at plasmon-waveguide chemical-sensor selectivity enhancement. The idea is to laminate the plasmon guide with another nanomembrane, incorporating artificial nanopores.[24] Use of synthetic gated-ion channels enables selective and switchable transport of analytes to the guide surface[25] and opens a pathway toward biomimetic enhancement of plasmonic structures.

In combination, artificial free-standing nanomembranes and plasmonics have opened up new research directions, further expanded by multifunctionalization. Nanomembranes can be used to fabricate stretchable and foldable plasmonic waveguides, circuits, and devices that are transferable to various substrates, including those that are curvilinear. They can be patterned and stacked to form 3D photonic and plasmonic crystals. They may be dynamically tuned through stretching and folding. They can be fabricated in various shapes, such as nanoribbons, and their properties can be engineered through multifunctionalization. There are many applications of nanomembrane guides—such as chemical and biological sensors—and photonic circuitry, such as active devices and photodetectors. Some functionalization approaches include those that are biomimetic, which facilitates the introduction of bionics into plasmonics. Available material choice even includes those that may be incompatible with biology. Possible limits are far away and are the subject of ongoing research.


Zoran Jakšić
Institute of Chemistry, Technology, and Metallurgy
University of Belgrade
Belgrade, Serbia

Zoran Jakšić received his PhD in electrical engineering from the University of Belgrade. His interests include nanophotonics, nanoplasmonics, and nano- and micro-electromechanical sensors and detectors. He has authored 210 peer-reviewed publications, including 46 journal papers. He is a full research professor.

True-color holograms may light up small displays

By Chris Lee | Last updated 9 days ago
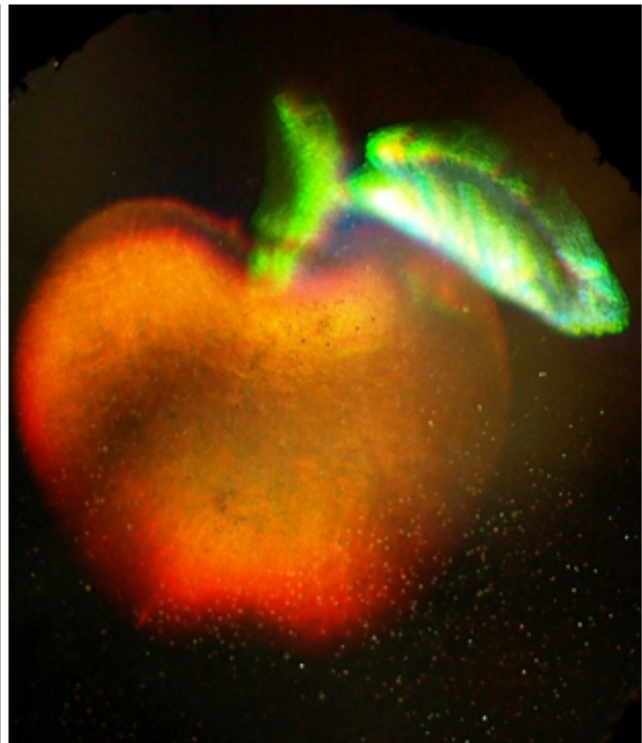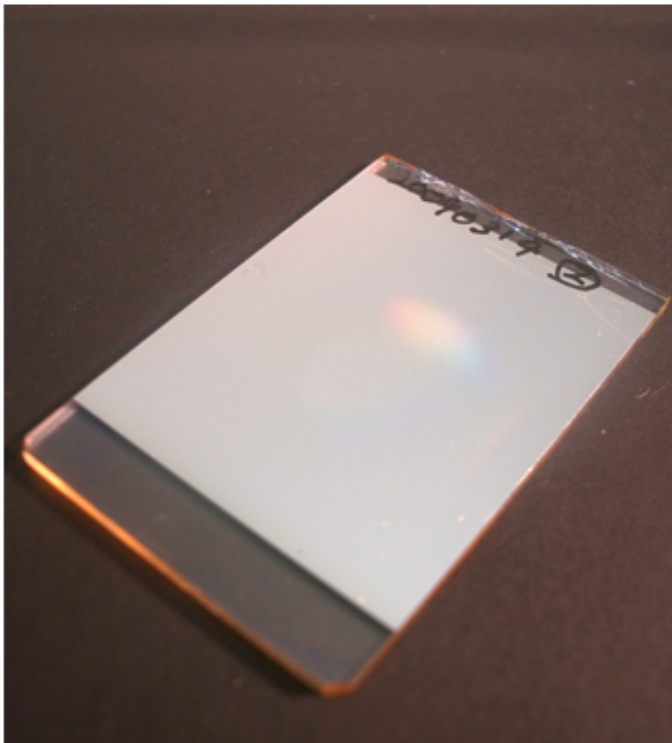
The recording media (left) and a resulting hologram
Science/AAAS

The Nintendo 3DS notwithstanding, 3D technology still comes under the classification of cumbersome. The viewing angle is usually poor, or you need to wear special glasses. Neither of these options are particularly attractive. An alternative is to use holograms, but this comes with its own set of problems. For instance, the holograms on credit cards are visible from a wide range of angles... but, well, they aren't called rainbow holograms for nothing. Holograms with better color reproduction have a limited viewing angle. All in all, it is rather fraught.

Riding to the rescue are engineers bearing surface plasmon polaritons. By combing some fairly standard holography techniques along with some surface plasmon polariton tricks, the researchers have created holograms that have both a wide viewing angle and good color reproduction.

So, how did they do it? First, a short primer on surface plasmon polaritons, entities that are part light and part electric charge. When light is incident on a metallic surface, it begins to move charges back and forth. Normally, this will result in the light being reflected from the surface. But charge motion can also become collective and begin to transit along the surface of the metal. When this happens, the light is not reflected—it's absorbed into the metal as a surface plasmon polariton.

To excite a surface plasmon polariton, we must match the speed of light *along the surface* to the speed of the surface plasmon polariton. This requires that we hit the surface at some angle that is not perpendicular to the surface, and because light in vacuum is just so damned fast, we have to slow it down. We do this by putting the metallic surface on some glass. This slows the light down by about 30 percent, allowing us to choose an angle of incidence and wavelength of light that will generate a surface plasmon polariton.

Having gotten a surface plasmon polariton into the metal, what do we do with it? We get it to radiate as light again. To do this, you pattern the metallic surface with a series of lines. These lines disrupt the movement of the surface plasmon polariton, causing it to emit light. However, the emission is in the form of a bunch of stripes that all add together to make a single bright spot at a single angle. By altering the lines, you could also create a pattern that doesn't allow the surface plasmon polariton to radiate at all, or allow red colors to radiate vertically, while green colors radiate at 45 degrees.

Having gotten a surface plasmon polariton into the metal, what do we do with it? We get it to radiate as light again. To do this, you pattern the metallic surface with a series of lines. These lines disrupt the movement of the surface plasmon polariton, causing it to emit light. However, the emission is in the form of a bunch of stripes that all add together to make a single bright spot at a single angle. By altering the lines, you could also create a pattern that doesn't allow the surface plasmon polariton to radiate at all, or allow red colors to radiate vertically, while green colors radiate at 45 degrees.

How does this relate to holograms? A hologram is recorded by mixing light that has bounced off an object with light that is undisturbed. The resulting fringe pattern records the amplitude and phase of the light associated with the object. These two bits of information are what gives a hologram its depth, in contrast to a normal photograph, which records the intensity of scattered light.

If this fringe pattern is recorded with different colors, the combined fringe pattern also records the colors that make up the object as well. The other thing to note is that a fringe pattern is just a bunch of lines that cross each other at various angles—just the sort of thing used to make a surface plasmon polariton radiate.

The researchers took advantage of this by recording their hologram on a metallic surface layered on a piece of glass. The cool thing is that if you illuminate the back of the glass plate with red, green, and blue lasers at the right angles, you end up with red, green, and blue surface plasmon polaritons traveling through the metal. These then hit the fringe pattern of the hologram—which, remember, records not just amplitude and phase, but color as well. The fringe pattern causes red colors to only be viewable in directions from which red was scattered in the original pattern. Likewise for green and blue, allowing for good color reproduction over the range of angles.

As with many things, this isn't all pixies and fairy dust. The angular range over which the hologram can be viewed with color accuracy is basically the same angular range over which the original hologram was illuminated, so to get a wide range of viewing angles, a number of holograms have to be overlapped. This makes the combination of wide viewing angle and accurate white balance very hard to achieve (but achievable all the same).

Furthermore, I suspect that the size of the image is rather small. While you might envision this as a display for something like a phone or a portable gaming system, it probably won't scale to a television display. On the technical development side, the researchers have shown static images, but display technology needs to be dynamic. They will need to develop a way to write the fringe patterns on the metallic substrate and erase them again in just a few milliseconds in order for this to progress to a workable 3D system. This last may well be a real barrier to any products and will require some innovative thinking.

Science NOW — UP TO THE MINUTE NEWS FROM SCIENCE

Holograms in True Color

by Sid Perkins on 7 April 2011, 2:01 PM | Permanent Link | 1 Comments

Email   Print | More   PREVIOUS ARTICLE   NEXT ARTICLE

Researchers have developed a new way to create true-color holograms that can be viewed from any angle using ordinary white light. The advance could lead to a new generation of electronic devices, such as cell phones or miniature televisions that display three-dimensional (3D) images.

True 3D images can be created in several ways. In the 1960s, researchers generated the first holograms by firing a laser at an object and then using a photosensitive material to record the pattern of interference between light waves reflected off the object and those striking the material directly from the laser. This hologram, if later illuminated with the same wavelength of laser light, reproduced a 3D (but monochromatic) image of the object. One well-known hologram of that era captured in red laser light a chessboard on which pieces could be viewed from various angles as a viewer shifted position.

The so-called rainbow holograms now common on credit cards are generated differently, using white light reflected off a silvery backing through a plastic film that contains several images, each stored in a different color in its own layer. As the hologram is viewed from different angles, the shifting view of those colored layers with respect to one another provide a 3D perspective. In many cases, the image produced by these rainbow holograms isn't a true-color representation of the object depicted.

Now, researchers report today in *Science* that they can create true-color holograms that can be viewed using only white light. Like the first holograms, the new technique uses lasers to generate an interference pattern, says Satoshi Kawata, a photonics physicist at Osaka University in Japan. To capture colors, Kawata and his colleagues illuminate the original object with three different lasers: red, blue, and green, the three primary colors of projected light. They store the hologram in a light-sensitive material coated with a thin layer of metal such as gold or silver, a veneer that contains free electrons that are easily excited when struck by radiation such as light waves.

To reproduce a 3D image, the researchers bathe the metal-sheathed material in ordinary white light, which contains all wavelengths of visible light (including red, blue, and green). That white light excites the free electrons; their resulting movements and oscillations (so-called surface plasmons) in turn give off light that regenerates the image—an image that combines the red, blue, and green versions of the hologram to generate a true-color representation of the original object. In their lab tests, Kawata and his colleagues created realistically hued holograms of an apple, a flower, a Japanese origami crane, and several other objects. For now, Kawata says, the new technique can produce only static holograms—no pint-sized Princess Leia pleading for help from Obi-Wan Kenobi just yet.

"It's quite a scientific achievement," says physicist Pierre-Alexandre Blanche of the University of Arizona in Tucson. The technique may be able to generate brighter images that can be seen through a broader range of viewing angles than holograms produced using other methods, adds media technologist V. Michael Bove Jr. of the Massachusetts Institute of Technology in Cambridge. The problem, he says, may be figuring out how to mass-produce images more cheaply than other techniques can.

Yet another issue may be scaling up the holograms to large size, says photonics physicist Nasser Peyghambarian of the University of Arizona. So far, the researchers apparently have created holograms only about the size of an index card. The prisms used to illuminate the holograms, which in the current scheme are mounted beneath or behind the metal-coated material, could easily become cumbersome in much larger displays, he contends.

Nevertheless, the notion of watching the Super Bowl on a coffee table with an embedded holographic display —complete with little linemen, wee wide receivers, even a tiny blimp floating a few feet above the potato chips and beer coasters—may someday become a reality to sports fans everywhere.

ENLARGE IMAGE
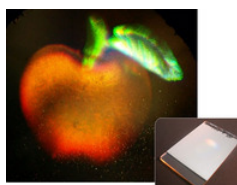
In living color. This three-dimensional, true-color image of an apple was generated using a new technique of making holograms (*inset*) that allows the image to be viewed using ordinary white light.

Credit: Science/AAAS

ScienceNOW. ISSN 1947-8062

Surface plasmons create vivid holograms

07 April 2011

Holograms displayed using interactions between light and the collective oscillations of electrons on the surface of a metal, known as surface plasmons, are set to transform three-dimensional imaging technology. Satoshi Kawata and his team from Japanese research insitute RIKEN's Saitama campus have constructed images that, unlike credit-card holograms, appear in the same natural colours from any angle.
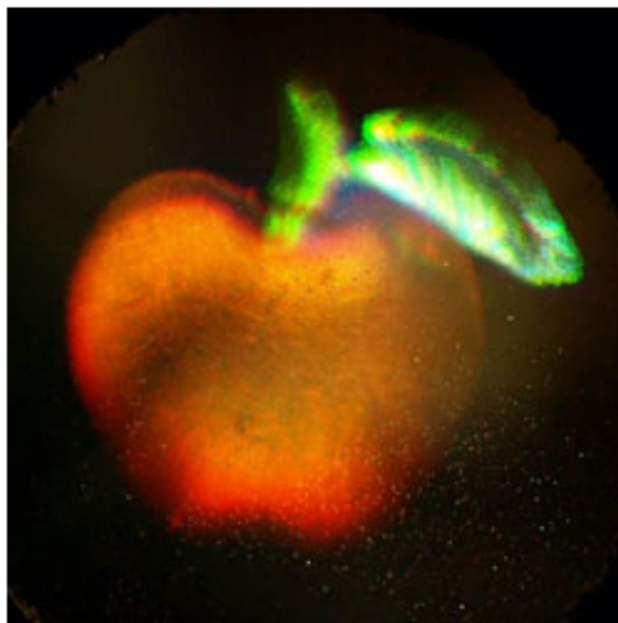
Plasmons are "quasiparticles" that are observed when electrons in a metal collectively oscillate at light wave frequency. If light falls on a metal with a lower frequency than the surface plasmons it is reflected, while higher-frequency light is transmitted. The frequencies of gold and silver's surface plasmons are in the visible range, causing their distinctive colours. Katawa's team exploits this phenomenon. 'Our proposal is plasmons can be used to select colours in a hologram,' he says. 'This hologram is reconstructed by white light - you don't need a laser.'

Lasers are still needed to make the hologram. Team members Miyu Ozaki and Jun-Ichi Kato illuminate objects with red, green and blue lasers and the light beams diffract onto a glass sheet covered in a 150 nm thick layer of photoresist material, recording the image.

To make the plasmon hologram, the scientists coated 55 nm silver and 25 nm glass layers onto the photoresist. Shining light into the hologram through a prism from three different angles, one for each colour, reconstructs the three-dimensional image.

Reconstruction of a red apple with a green leaf in three dimensions using surface plasmon holograms

© Science/AAAS

Katawa predicts that he and other scientists will eventually use this method to create moving pictures. But even before that such holograms promise 'revolutionary' tools for personalised medicine, according to Heike Arnolds, who researches plasmon-enhanced photochemistry at the University of Liverpool. 'Chemists are ideally placed to exploit this by producing functionalised hologram surfaces for surface plasmon resonance sensors,' she says. A glucose sensor might display its readout through characteristic colour changes, Arnolds explains. 'If your apple doesn't look green, go see a doctor.'

Andy Extance

Interesting? Spread the word using the 'tools' menu on the left.

References

M Ozaki *et al*, *Science*, 2011, DOI: 10.1126/science.1201045

Click here to print

MailOnline

# Scientists 'prove' that time travel will always be impossible by building a toy version of the Big Bang

By **Daily Mail Reporter**
Last updated at 10:57 AM on 14th April 2011

If you've long harboured a fantasy of firing up the Delorean and becoming the next Marty McFly, then sadly it looks like your time-travelling dreams have finally been dashed.

For scientists at the University of Maryland claim to have proved that time travel is impossible and will forever remain a Hollywood invention.

Igor Smolyaninov and Yu-Ju Hung have built a toy version of the Big Bang - the point at which the universe was created around 13.7 billion years ago.
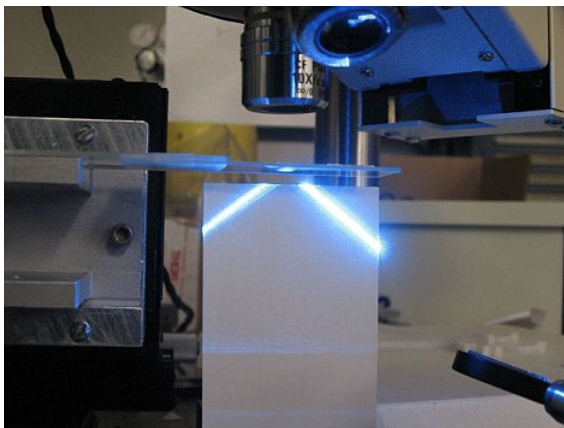
**Going out with a bang: Scientists in the U.S. claim their experiment proves time travel is impossible**

The desktop experiment simulates how light and timed flowed during the Big Bang - but not the explosion itself.

According to the research, it could help explain why time only marches forward and disorder increases - why we only get older not younger and why a smashed plate cannot become unbroken.

In a report in Physical Review Letters, Smolyaninov describes their work as 'simple experimental geometry'.

For the experiment, researchers took strips of acrylic and gold called metamaterial, and arranged them to twist light in unusual ways.

These substances can be thought of as 'invisibility cloaks', bending light around objects to disguise them.
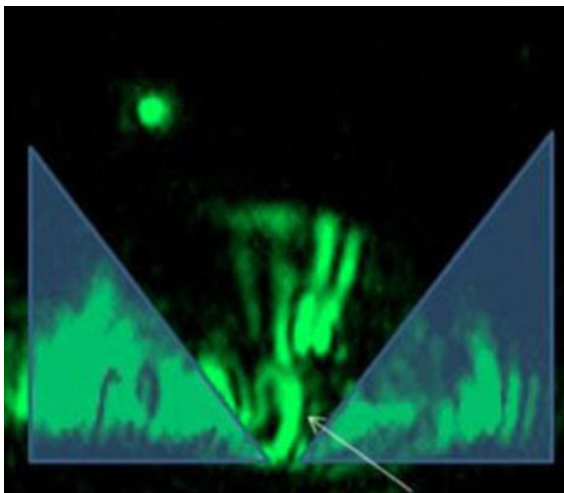

Shed some light: An image from inside 'Big Bang-in-a-box'

It has also been claimed that metamaterial can mimic astronomical events such as a planet orbiting a star or how light behaves in a black hole.

When a laser hit the metamaterial, it excited waves of plasmons on the surface - which appeared to only move in one direction.

The movement is the same as how massive particles move through time and space - creating a Big Bang-like moment.

At first the scientists believed they could create time travel - by building a metamaterial in which light moving in a circle was mathematically identical to particles moving through time, then sending a plasmon on a circular orbit bringing it back to the same point it started.
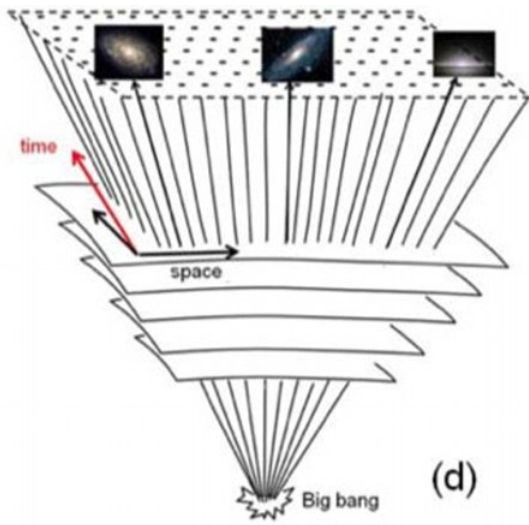
Mystery solved? A diagram of the Big Bang

© Universal Pictures/Photofest

No firing up the Dolorean: Christopher Lloyd as Doc Brown and Michael J Fox as Marty McFly in the film Back To The Future

But it turns out to be even more complicated than that - for the specific light that is need to interact with particles travelling through time cannot go in a circle.

'Time travel in this model looks like it's impossible,' said Smolyaninov.

However the research team did acknowledge that the the experiment was not absolute in its findings.

'It will never give you the real final answer about the real Big Bang and real time,' said Smolyaninov. 'But if you study it, you may discover something, and you may be able to ask more intelligent questions.'

For example, it could help scientists understand more about the 'Big Crunch' - one scenario on the fate of the universe when the constant expansion of light and time from the Big Bang reverses and the universe collapses into a black hole.

Comments (46)

- Newest
- Oldest
- Best rated
- Worst rated

View all

Teddy Robbear - I refuse to believe you have a PhD of any value when I read the utter nonsense you spout on here about a fairy in the sky. No educated man has faith in a made-up god in the way you do. Someone with a PhD, by definition a research degree would surely have educated himself on the details of the bible and found them to be false, as did I? - Norma Lee Lucid, Wigan, UK, 15/4/2011 Many scientists and other academics and professionals lead lives of religious practice and faith and yet engage fully with the physical, medical, and social sciences and the worlds of politics and literature. Such people are rational and thoughtful and skeptical. They are critical thinkers.

- Teddy Robbear PHD, Scotland, 17/4/2011 21:15

Click to rate ˌ ˌ Rating   4

Report abuse

Read Brian Cox's wonderful book "Why Does E=mc2 (And why should we care?)". To move in any other direction in space-time requires that we move faster than the speed of light. Unless that is possible (and it isn't) we cannot travel backwards in time, only forward. - Simon, Bath, 15/4/2011 12:12 I prefer his "Things can only get better" song to his science. He's a typical attention seeking individual with a false Blair like smile which is ok for your average pop star but not your scientists, who are best heard and not seen. Good looking people make bad scientists, because no one is listening to them, just remarking on how good looking he is.

- Teddy Robbear PHD, Scotland, 17/4/2011 21:08

Click to rate ˌ ˌ Rating   5

Report abuse

Total rubbish. I drive fast and still have a 70s hair style! The big crunch and time reversing is also bunkum. Even Stephen Hawking acknowledged that. Time doesn't reverse just because you're going backwards.

- rupert, Yorkshire, UK, 17/4/2011 18:27

Click to rate ˌ ˌ Rating   4

Report abuse

What a load of rubbish! everybody knows you can time travel by hitting 88MPH

04/06/2011

Metamaterial Reveals Nature of Time and the Impossibility of Time Machines

By recreating the Big Bang inside a metamaterial for the first time, physicists have shown why the cosmological arrow of time points in the same direction as the thermodynamic arrow of time

By kfc
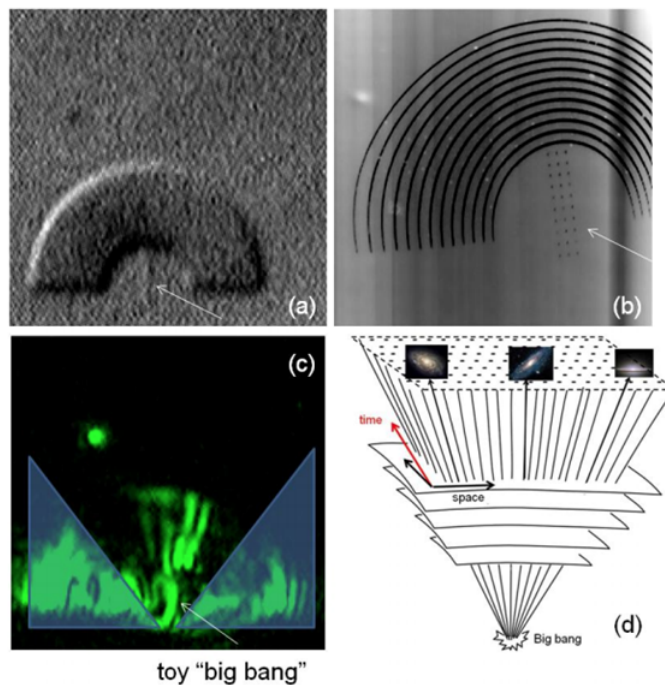
toy "big bang"

Metamaterials are periodic structures that can be engineered to steer light in specific ways. The trick is to manipulate the properties of the "electromagnetic space" in which light travels by controlling the values of the permittivity and permeability of this space.

In recent years, physicists have had a great deal of fun using metamaterials to build all kinds of exciting devices, the best known being invisibility cloaks which steer light around an object, thereby concealing it from view.

But metamaterials have a more profound application because there is a formal analogy between the mathematics of electromagnetic spaces and the mathematics of general relativity and the spacetime it describes.

That means it is possible to reproduce inside a metamaterial an exact copy of many of the features of spacetime. We've looked at a number of these ideas, such as how to build a black hole and even create a multiverse.

Today, Igor Smolyaninov at the University of Maryland, College Park, says it is possible to recreate the arrow of time inside a metamaterial. Such an experiment, he says, allows the experimental study of one of the great outstanding mysteries in science: why the cosmological arrow of time is the same as the thermodynamic arrow of time.

At the same time, the exercise gives a curious insight into the potential for time travel.

The arrow of time is a long standing puzzle. Many cosmologists believe that the Universe began with the Big Bang, an event that is clearly in our past.

And yet our standard definition of time comes from thermodynamics and the observation that entropy always increases with time. For example, you can easily break an egg or mix milk into your tea but reversing these processes is hard. Observing phenomena like these defines the arrow of time.

But why should the cosmological and thermodynamic arrows of time point in the same direction?

Metamaterials can help researchers study this problem because it is possible to manipulate them so that space-like dimensions become time-like. Smolyaninov describes how to create a material in which the the x and y directions are space-like while the z-direction is time-like.

The way light moves in this space is exactly analogous to the behaviour of a massive particle in a (2+1) Minkowski spacetime, which is similar to our own universe. So the pattern of light

propagation inside this metamaterial is equivalent to the "world lines" of a particle in a Minkowski universe.

Smolyaninov says that a Big Bang event in the metamaterial occurs when the pattern of light rays expands relative to the z-dimension, or in other words, when the world lines expand as a function of time. This establishes a cosmological arrow of time.

The next question is how this arrow relates to a thermodynamic arrow of time. This requires a definition of entropy inside the metamaterial which Smolyaninov says is a kind of measure of the disorder associated with the light rays.

If the metamaterials are perfect the rays should propagate perfectly. But they're not perfect and so distort the rays as they spread. This determines a thermodynamic arrow of time and shows why it is the same as the cosmological arrow of time.

But there's a problem of course. Although there is a formal mathematical analogy between these spaces, it's not at all clear what plays the role in Minkowski space of the imperfect propagation of light through electromagnetic space.

In the past, scientists have only been able to think about these problems theoretically but metamaterials now allow them to s study them experimentally.

Amazingly, Smolynainov and a colleague, Yu-Ju Hung, have actually built their time simulator. Their system is made using specially shaped plastic strips placed on a gold substrate. And the light rays are actually plasmons that propagate across the surface of the metal while being distorted by the plastic strips.

This represents a number of firsts. To start with, Smolyaninov uses this system to recreate the Big Bang in his lab. He calls it a toy Big Bang but it's hard to understate the significance of this event. A Big Bang in your own lab!

He then goes on to use his model to study the arrows of time. Imagine: your own custom-built arrow of time!

This system also gives an interesting insight into the nature of time machines. The question Smolyaninov asks is whether it is possible to create closed time-like curves in his material. This is equivalent to asking whether it is possible for particles in a Minkowski space to travel in a curve that takes them back to the point in space-time where they started.

He considers this by imagining a cylindrical metamaterial in which the z-dimension and radial dimension are space-like and the angular distance around the cylinder is time-like. Can closed time-like curves exist in this system, he asks. "At first glance, this question is simple, and the answer should be "yes"," he says.

But under closer examination the answer turns out to be different. He points out that while it is possible for light rays to follow circular paths that return to the point from where they started, these rays would not perceive the angular dimension as time-like.

By comparison, any ray that does perceive the angular dimension as time-like cannot actually return to the same point in space-time, (although it can travel a world line that is very close to a closed time-like curve). So time machines, even trivial ones like this, are impossible.

That's hugely impressive work. Smolyaninov is one of the world's leading thinkers on metamaterials and has done much to advance the theory that links electromagnetic and Minkowski spaces.

Now he's actually getting his hands dirty. In creating for the first time metamaterials that reproduce the Big Bang and the arrows of time that result, he's surely achieved an extraordinary landmark.

Ref: arxiv.org/abs/1104.0561: Modeling of Time with Metamaterials

You can now follow The Physics arXiv Blog on Twitter
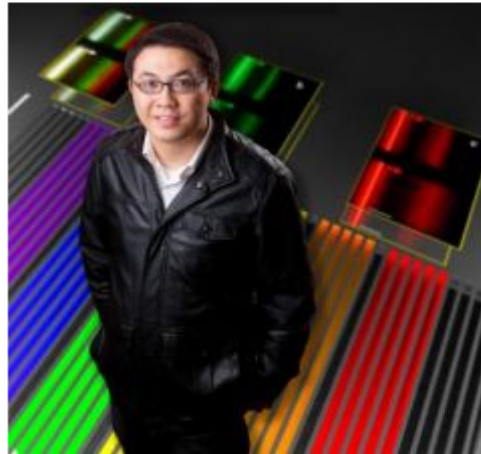
Plasmonic Structures Trap a Rainbow

WRITTEN BY NANCY LAMONTAGNE | 20 APRIL 2011

SHARE

Researchers at the State University of New York (SUNY) at Buffalo and Lehigh University have theoretically and experimentally described trapping light of different wavelengths in a single nanoplasmonic structure.

Trapping multiple wavelengths of light could be useful for increasing the optical absorption of solar cells. Qiaoqiang Gan, an Assistant Professor from SUNY at Buffalo's School of Engineering and Applied Sciences, and his colleagues in Filbert Bartoli's group at Lehigh University created plasmonic structures by making nanoscale grooves in metallic surfaces at different depths, which led to altering the materials' optical properties.

Nanomaterials created by Qiaoqiang Gan allow for the trapping of different wavelengths of light. Credit: Douglas Levere, UB Communications

The optical properties of the nanoplasmonic structures allow different wavelengths of light to be trapped at different positions in the structure, trapping multiple wavelengths on a single chip. Conventional methods (e.g. ultra cold gas) can only trap a narrow spectral band. The engineered surface of the nanostructures allow plasmon resonances, where light excites the waves of electrons that oscillate back and forth on metal surfaces. The structures can provide the interface between photons and electrons that is critical for enhancing performance in optical computing as well as photovoltaic devices.

The nanoplasmonic structures can trap slow resonances of light at room temperature. This results in a great improvement over the ultra cold temperatures required in conventional slow-light technologies. "In the *PNAS* paper, we showed that we trapped light from the visible red to the visible green," explained Gan. "Now we are working on trapping, the entire rainbow from the visible red to the visible blue," Gan said.

Gan cautions that there is still a long way to go before the structures could be useful for photovoltaic devices. Various research groups are investigating nanostructures to support surface plasmon waves and are developing applications, including plasmonic-enhanced photovoltaic devices, based on these nanostructures. Like many of these groups Gan's team is working to improve their structures' coupling efficiencies. "This is the biggest challenge we are facing to employ our structure to practical solar cells. Currently, we employ a simple nanoslit to couple the light to surface plasmon waves, whose coupling efficiency is weak," Gan said.

They are considering various ways of optimizing the coupling mechanism. End-fire coupling, for example, might enhance the coupling efficiency between the incident light and surface plasmon modes. "If this coupling efficiency challenge could be overcome in the near future, our structures should be promising for planar thin-film solar cells," he said. One way it could be used would be to combine the graded structure with solar cells to allow trapping of different wavelengths within the active layer of an organic photovoltaic device.

Research paper: Experimental verification of the rainbow trapping effect in adiabatic plasmonic gratings, *PNAS* Vol. 108, No. 13, pp. 5169-5173.

Rainbow-Trapping Scientist Now Strives to Slow Light Waves Even Further

An electrical engineer at the University at Buffalo, who previously demonstrated experimentally the "rainbow trapping effect" -- a phenomenon that could boost optical data storage and communications -- is now working to capture all the colors of the rainbow.

In a paper published March 29 in the Proceedings of the National Academy of Sciences, Qiaoqiang Gan (pronounced "Chow-Chung" and "Gone"), PhD, an assistant professor of electrical engineering at the University at Buffalo's School of Engineering and Applied Sciences, and his colleagues at Lehigh University, where he was a graduate student in Dr. Filbert Bartoli's group, described how they slowed broadband light waves using a type of material called nanoplasmonic structures.

Gan explains that the ultimate goal is to achieve a breakthrough in optical communications called multiplexed, multiwavelength communications, where optical data can potentially be tamed at different wavelengths, thus greatly increasing processing and transmission capacity.

He notes that it is widely recognized that if light could ever be stopped entirely, new possibilities would open up for data storage.

"At the moment, processing data with optical signals is limited by how quickly the signal can be interpreted," he says. "If the signal can be slowed, more information could be processed without overloading the system."

Gan and his colleagues created nanoplasmonic structures by making nanoscale grooves in metallic surfaces at different depths, which alters the materials' optical properties.

These plasmonic chips provide the critical connection between nanoelectronics and photonics, Gan explains, allowing these different types of devices to be integrated, a prerequisite for realizing the potential of optical computing, "lab-on-a-chip" biosensors and more efficient, thin-film photovoltaic materials.

According to Gan, the optical properties of the nanoplasmonic structures allow different wavelengths of light to be trapped at different positions in the structure, potentially allowing for optical data storage and enhanced nonlinear optics.

The structures Gan developed slow light down so much that they are able to trap multiple wavelengths of light on a single chip, whereas conventional methods can only trap a single wavelength in a narrow band.

"Light is usually very fast, but the structures I created can slow broadband light significantly," says Gan. "It's as though I can hold the light in my hand."

That, Gan explains, is because of the structures' engineered surface "plasmon resonances," where light excites the waves of electrons that oscillate back and forth on metal surfaces.

In this case, he says, light can be slowed down and trapped in the vicinity of resonances in this novel, dispersive structural material.

Gan and his colleagues also found that because the nanoplasmonic structures they developed can trap very slow resonances of light, they can do so at room temperature, instead of at the ultracold temperatures that are required in conventional slow-light technologies.

"In the PNAS paper, we showed that we trapped red to green," explains Gan. "Now we are working on trapping a broader wavelength, from red to blue. We want to trap the entire rainbow."

Gan, who was hired at UB under the UB 2020 strategic strength in Integrated Nanostructured Systems, will be working toward that goal, using the ultrafast light source in UB's Department of Electrical Engineering in the laboratory of UB professor and vice president for research Alexander N. Cartwright.

"This ultrafast light source will allow us to measure experimentally just how slow is the light that we have trapped in our nanoplasmonic structures," Gan explains. "Once we know that, we will be able to demonstrate our capability to manipulate light through experiments and optimize the structure to slow the light further."

Co-authors with Gan on the study are Filbert Bertoli, Yongkang Gao, Yujie Ding, Kyle Wagner and Dmitri Vezenov, all of Lehigh University.

The University at Buffalo is a premier research-intensive public university, a flagship institution in the State University of New York system and its largest and most comprehensive campus. UB's more than 28,000 students pursue their academic interests through more than 300 undergraduate, graduate and professional degree programs. Founded in 1846, the University at Buffalo is a member of the Association of American Universities.
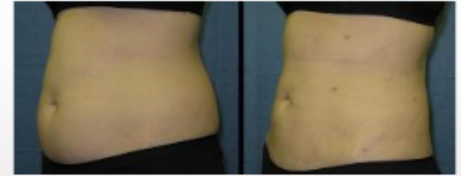
Sensitive label-free DNA sensing based on metal/fluorophore interactions

(*Nanowerk News*) With two recent studies, imec scientists contribute to the field of label-free DNA sensing. The measurement technique they have refined is based on the fact that metallic films and nanoparticles absorb the light of nearby light-emitting fluorophores. In one study, the quenching and enhancement of the emitted light was studied and quantified with a wide range of gold nanoparticles and DNA hairpin probes. In a second study and using similar probes, the technique was used to demonstrate a functional label-free genosensor.

Metals are ultra-efficient quenchers of light-emitting fluorophores. When fluorophore molecules are located within a few nanometers from a metal surface, their fluorescence signal is suppressed. When they are moved further away from the metal (e.g. by some spacer molecule), an enhanced fluorescence signal is measured. This phenomenon of clearly distinct quenched and enhanced signals can be used for biosensing applications such as DNA detection.
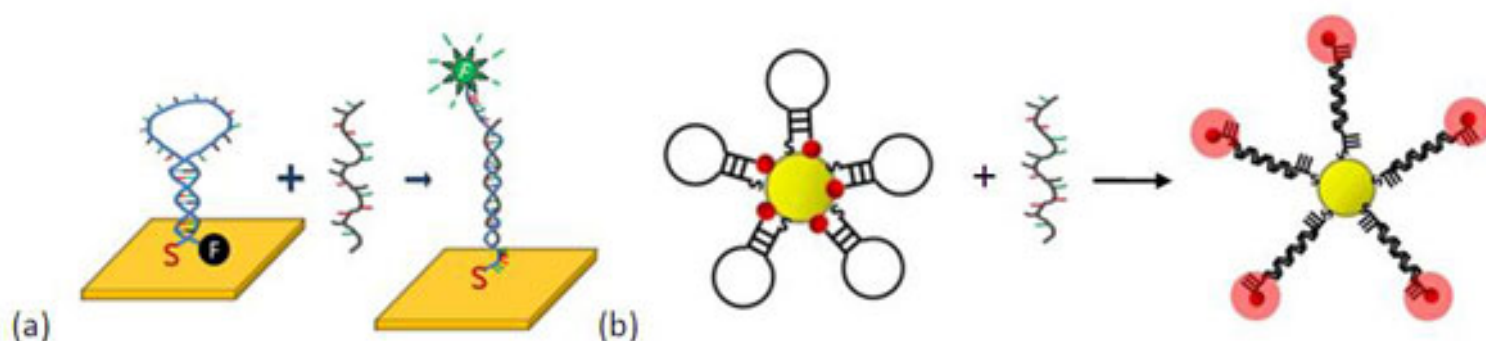
DNA sensing

DNA hairpin probes are single-stranded DNA sequences that are folded through their outer ends that bind to each other. The middle part of the strands is complementary to the DNA sequence that we want to detect. Here we used hairpin probes that have at one end a fluorophore molecule attached while at the other end they are bound to the metal surface (gold). In the absence of the target DNA sequence, the hairpin remains closed and the fluorophore is close to the metal. But when the DNA sequence of the hairpin meets its complimentary strand, the strands hybridize and the hairpin opens. At that moment, the fluorophore molecule is further away from the metal, resulting in an enhanced fluorescence signal.

In one study, we examined fluorescence quenching and enhancement near gold nanoparticles of various sizes, and with DNA hairpin probes of different lengths. As a result, we report a 96.8% quenching efficiency for all particles sizes tested, and a more than complete signal recovery after DNA hybridization. Initial sensing experiments indicate a detection sensitivity of 100pM and below. Previous studies had not been able to relate light quenching and enhancement to the number of fluorescence molecules involved. We were able to quantify the number of fluorophores attached to DNA hairpin probes using a novel thiol exchange method. This allowed us to examine and quantify both the quenching efficiency and enhancement factor.

In a second development, we made a label-free genosensor based on DNA hairpins immobilized on a gold surface under microfluidic conditions. We used a microfluidic integrated instrument based on surface plasmon resonance combined with a gold chip. This instrument was first used to immobilize the DNA-fluorophore hairpins and then to promote the hybridization of the target molecules. The fluorescent signal was visualized with fluorescence microscopy. We experimented with the various design options of this sensor, investigating the detection sensitivity and specificity. With our resulting sensor, we reached a detection sensitivity of 300pM.

This article printed from:

PharmaDiagnostics¹ SoPRano wins prestigious product award at SBS 2011

Label-free assay technology receives New Product Award Designation from panel of scientific and industry specialists

Brussels, April 12, 2011- PharmaDiagnostics NV, a company developing and marketing a broadly-enabling, label-free screening technology that uniquely does not require specialized equipment, announces today that their SoPRano(TM) technology has won its third award in 12 months. SoPRano was awarded an SLAS (Society for Laboratory Automation and Screening) New Product Award (NPA) Designation at SBS 2011, the conference and exhibition highlighting pharmaceutical and biomolecular screening technologies in Florida March 27 – 31, 2011.

PharmaDiagnostics' SoPRano technology was awarded the NPA Designation by a panel of scientific specialists chaired by Al Kolb of KeyTech Solutions, and including Charles Lunn of Merck and Ricardo Macarron of GSK. SoPRano was selected for the prize from a large range of products at the exhibition at which 155 different companies were exhibiting.

The yearly SBS conference is organized by the Society for Laboratory Automation & Screening (SLAS), an international community of more than 10,000 individual scientists, engineers, researchers, technologists and others from academic, government and commercial laboratories. SLAS provides forums for education and information exchange to encourage study and advance laboratory science and technology for the drug discovery, agrochemical, biotechnology, chemical, clinical diagnostic, consumer product, energy, food, forensic, pharmaceutical, security and other industries.

This is the third time in the last 12 months that PharmaDiagnostics SoPRano has won a first prize technology award at a leading exhibition. In addition to the prize at SBS 2011, PharmaDiagnostics also won the ELRIG Technology Prize twice in 2010. This was at Drug Discovery 2010, Coventry, in September 2010 and Liquid Handling & Label Free Technologies 2010 in March 2010.

Label-free screening is an area of great interest and potential growth in pharmaceutical research. To date, the expanding SPR segment of this market has been dominated by providers of expensive specialist instrumentation that is unable, due to technical constraints, to provide the throughput required for routine adoption of label-free screening. PharmaDiagnostics' SoPRano label-free platform is the first SPR-based system to utilize standard plate-readers, and simple assay protocols. This makes for increased accessibility for researchers, lowers barrier to adoption and also offers excellent scalability, thus lowering costs, as it is not necessary to increase instrument expenditure to increase throughput.

"Winning our third prize in 12 months, this time from the SBS 2011 conference at which we are assessed against many multinational suppliers, is continued demonstration that SoPRano's appeal to industry and academic experts is real and ongoing," said Dr David Ricketts, CEO at PharmaDiagnostics. "SoPRano was chosen by a select panel of well respected industry figures. This prize at the SBS conference is further proof that the potential of a label-free platform that requires no expensive instrumentation, and offers high throughput, is recognized by key members of the industry."

About PharmaDiagnostics NV

PharmaDiagnostics NV develops label-free screening technology with the unique capability in its market of operating without the need for specialized hardware. The technology is broadly enabling and applicable to a range of applications including: receptor-ligand binding; enzymatic reactions; antibody screening and ADME. The assays are very sensitive and have the potential for very high throughput. The company is focused upon licensing its technology for use in pharmaceutical and biotechnology companies, and also offers bespoke assay development services. In addition the company is seeking collaborations to develop applications in compound screening, particularly fragment screening and antibody screening. PharmaDiagnostics' novel technology platform, SoPRano(TM), is based on localized surface plasmon resonance (LSPR) and noble metal nanoparticles, and is run on standard laboratory equipment.

The company, based in the Z1 Research Park in Zellik, near Brussels, was founded in 2007. It has raised more than EUR 4.0 million (USD 5.6M) in two rounds of venture funding and EUR 100,000 in grants from IWT (Instituut voor de aanmoediging van innovatie door Wetenschap & Technologie in Vlaanderen), a Flemish innovation agency.

For further information, please contact: Andrew Lloyd & Associates Andrew Lloyd / Neil Hunter Tel: +44 1273 675100 allo@ala.com / neil@ala.com
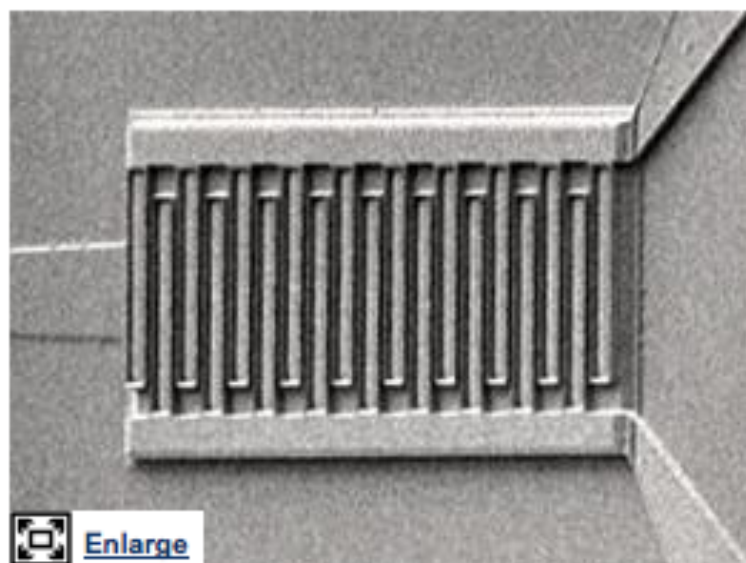
Electron resonances could greatly enhance the response of optical chip photodetectors

March 28, 2011 By Lee Swee Heng

article	comments (0)		share

Scanning electron microscopy image of the germanium-silicon-based photodetector with metal contacts to induce plasmonic light enhancement. Credit: 2010 AIP

Enlarge

Optical chips are the latest innovation in silicon technology with the potential to revolutionize telecommunications. Their operation relies on several key components, including light-emitting devices, waveguides and photodetectors. Engineers are looking for ways to miniaturize these components without sacrificing the data-processing speed of the integrated optical chips. Patrick Guo-Qiang Lo and co-workers at the A*STAR Institute of Microelectronics have now fabricated a highly sensitive photodetector by exploiting the enhancement effects of electron resonances that occur at metal contacts.

Surface plasmon polaritons—the collective movements of electrons at the surface of metals—are known to enhance and focus electromagnetic waves in their vicinity. The plasmon effect has been studied extensively for its ability to enhance the performance of optical devices, but in this study the researchers applied the phenomenon to improved the sensitivity, and hence speed, of semiconductor detectors.

Photodetectors on a silicon chip are generally designed to pick up light arriving through silicon waveguides. The light travelling through the silicon waveguides is detected by germanium, another semiconductor, which is grown directly on top of the silicon structure. However, the sensitivity of the germanium detector needs to be enhanced considerably in order to increase the speed and reduce the footprint of the photodetector further.

Plasmonic resonances can easily enhance the sensitivity of this light detection. The researchers introduced plasmons by adding thin aluminum contacts on top of the device (pictured). The plasmonic effects in the metal films channel considerably more light from the silicon waveguide into the photodetector, with important implications for device performance. "The enhanced photodetection enables the use of smaller devices, which in turn means that the device speed can be increased considerably," explains Lo.

The researchers demonstrate detection speeds of 37.6 picoseconds or faster, corresponding to a data transmission speed of 11.4 gigahertz—several orders of magnitude faster than that achievable by current broadband connections.

At the same time, these speeds still lag behind the full potential of these detectors. One of the reasons, says Lo, is loss that arises from the plasmonic resonances, which absorb some of the light and therefore reduce the amount of light that arrives at the detector. "The response of the detector is lower than what we expected from our design," says Lo. "Enhancing the plasmonic properties of the detector, for example through the design of different geometries, could alleviate such problems and enable a further miniaturization of photodetectors on silicon chips."

The A*STAR-affiliated researchers contributing to this research are from the Institute of Microelectronics

Researchers report a novel nanoscale integrated all-optical diode

(*Nanowerk News*) Recently, new achievements were made in the integrated optics by the Creative Research Group of Femtosecond Photophysics & Integrated Optics at Peking University. The group realized a novel nanoscale integrated all-optical diode having ultralow power and ultrahigh transmission contrast after the realization of the all-optical switch device with ultralow power and high-speed photonic crystal.

The related research paper, titled "Low-Power and High-Contrast Nanoscale All-Optical Diodes Via Nanocomposite Photonic Crystal Microcavities", has been published in the journal *Advanced Functional Materials*.

The photonic crystal all-optical diode is one of the important integrated photonic devices, which has potential applications in the fields of optical computing, optical interconnection systems, and integrated photonic circuits. Low operating power and high transmission contrast are the two key characteristics for the photonic crystal all-optical diodes. Owing to the relatively small nonlinear optical coefficients of the conventional optical materials, the operating threshold power is rather high with a threshold intensity of several hundred GW / cm2. Moreover, the transmission contrast was achieved only less than 100. This has greatly restricted the practical applications of the photonic crystal all-optical diodes.

By combining the strong plasmonic response of metal nanoparticles and the strong photon confinement effect of photonic crystal microcavity, the group has constructed a nanocomposite photonic crystal microcavity with very large third-order nonlinear susceptibilies. A prototype device of photonic crystal all-optical diode is realized based on the effect of surface-plasmon resonance enhancing optical nonlinearity and dynamic coupling of asymmetrical microcavity modes. An ultralow threshold photon intensity of 2.1 MW / cm2 and an ultrahigh transmission contrast of 11875 are achieved simultaneously. Compared with previously reported all-optical diodes, the operating threshold power is reduced by four orders of magnitude, while the transmission contrast is enlarged by three orders of magnitude.

The research achievement will not only promote the practical application research on the integrated photonic devices like all-optical diodes, but also provide a new approach for the study of nonlinear optical material.
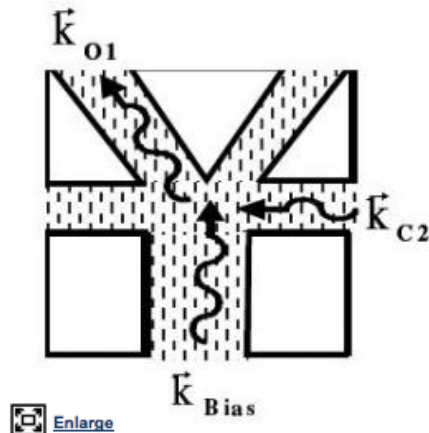
New Digital 'Electronics' Concept May Continue Moore's Law

November 5, 2009 By Lisa Zyga   • feature

article	comments (12)		share

In the NFL logic device, the first SPW (kBias) is launched, followed by the launch of a second SPW (kC2), which steers the first SPW into the left drain terminal for detection, where it's identified as a logic "1". Image copyright: De Los Santos. ©2009 IEEE.

Enlarge

(PhysOrg.com) -- Computers of the future could be operating not on electrons, but on tiny waves traveling through an electron "fluid," if a new proposal is successful. The new circuit design, recently introduced by Dr. Héctor J. De Los Santos, CTO of NanoMEMS Research, LLC, in Irvine, California, may be a promising candidate to replace CMOS-based circuits, and ultimately continue the circuit density growth described by Moore's Law.

As Gordon Moore predicted more than 40 years ago, the number of transistors able to fit on a computer chip has doubled approximately every 18 months. But if the trend is to continue for the years to come, it will have to be with technology other than the conventional CMOS design. As the size of transistors gets down to the nanoscale, CMOS devices begin suffering from several issues, such as increased resistance, decreased channel mobility, and increased manufacturing costs.

To overcome the challenges involved with scaling, researchers from around the world have begun to look for alternatives to CMOS technology. De Los Santos' concept, called nano-electron-fluidic logic (NFL), is based on the flow of plasmons in a fluid-like electron gas (basically an electron fluid). He predicts that logic gates with the NFL design offer the potential for femtosecond switching speeds and sub-femtojoule power dissipations at room temperature - numbers that would be extremely capable of continuing Moore's Law beyond CMOS. De Los Santos' paper will be published in a future issue of *IEEE Transactions on Nanotechnology*.

As De Los Santos explains, the NFL concept takes advantage of the properties of surface plasma waves (SPWs). These waves propagate on the inversion layer at the insulating gate-semiconductor interface (which, in this case, embodies an electric fluid) and behaves as an SPW waveguide. When two SPWs collide, they repel each other. In the device set-up, one SPW is launched from a particular direction to collide with another SPW, causing it to scatter in one of two directions, where it is detected and interpreted as a "1" or, if not detected, a "0."

To begin the process, an SPW is launched into a channel filled with electron fluid that forks into two channels, each with a detector at the end. Under no external forces, the SPW will be split equally so that equal portions will be detected at the two end terminals. But when a second SPW is launched into the main channel from the left or right, it will cause the original SPW to deflect into the opposite fork. For example, a second SPW coming from the right would steer the original SPW down the left fork. When the SPW is detected at the left end terminal, and not the right, the NFL device forms the basis of a logic flip-flop, having the ability to store one bit of memory.

Quantum dots enable plasmonic semis

R. Colin Johnson

4/19/2011 1:08 AM EDT

PORTLAND, Ore.—Plasmonic semiconductors will revolutionize electronics by allowing the easy coupling of photons (light) and electrons, according to researchers at the U.S. Department of Energy (DOE) Lawrence Berkeley National Laboratory.

Plasmons are wavefronts that couple independent electrons together into quasi-particles that travel in waves on a surface, allowing their frequency to be matched to that of incident photons, thus coupling electronic plasmons with optical photons at resonance. Achieving such localized surface plasmon resonance in a semiconductor is predicted by Berkeley Lab enable electronic interconnects where signals are sped up to the speed of light, **on-chip lenses for lasers and sensors,** a new generation of super-efficient **plasmonic light-emitting diodes (LEDs),** a new generation of supersensitive chemical and biological detectors, as well as metamaterials that can bend light around object to create an invisibility cloak.

Comment

4/19/2011 2:25 PM EDT
A longer article from Berkeley Lab is at ...
More...

Brad Pierce

More Comments >

Until now plasmonic devices were based on interfaces between metals and insulators (dielectrics), but these new results claim that many common semiconductors can also be crafted to transport plasmons, according to Berkeley Lab, which reported achieving surface plasmon resonances in vacancy-doped semiconductor nanocrystals—quantum dots.

"Doped semiconductor quantum dots open up the possibility of strongly coupling photonic and electronic properties, with implications for light harvesting, nonlinear optics, and quantum information processing," said Berkeley Lab Director Paul Alivisatos.

Surface plasmon resonances from p-type carriers in vacancy-doped copper-sulfide dots used quantum confinement to tune the electronic properties to the near-infrared range of the electromagnetic spectrum. The strong coupling between the photonic and electronic modes, the researchers claim, could be used to greatly enhance the exciton-light interactions of solar photovoltaics and artificial photosynthesis. Next, the team is experimenting with copper selenide and quermanium telluride semiconductors, to measure the expected enhancements in solar cells and memory devices made with them, respectively.
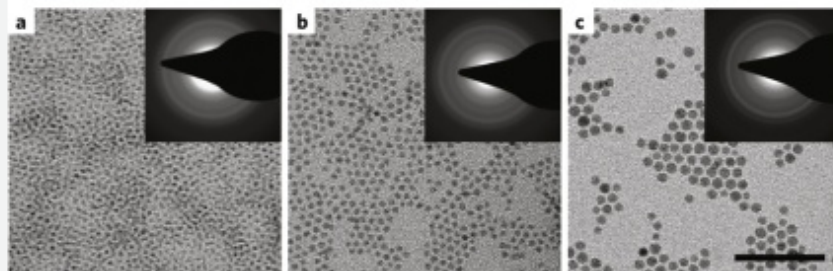
Transmission electron micrograph (TEM) shows electron diffraction patterns (inset) of three quantum dot samples with average size of (a) 2.4 nanometers (b) 3.6 nm, and (c) 5.8 nm. *Source: Lawrence Berkeley National Laboratory*

New Kid on the Plasmonic Block

By: Other Author - Published: April 18 2011

Berkeley Lab Researchers Find Plasmonic Resonances in Semiconductor Nanocrystals

With its promise of superfast computers and ultrapowerful optical microscopes among the many possibilities, plasmonics has become one of the hottest fields in high-technology. However, to date plasmonic properties have been limited to nanostructures that feature interfaces between noble metals and dielectrics. Now, researchers with the U.S. Department of Energy (DOE)'s Lawrence Berkeley National Laboratory (Berkeley Lab) have shown that plasmonic properties can also be achieved in the semiconductor nanocrystals known as quantum dots. This discovery should make the field of plasmonics even hotter.

"We have demonstrated well-defined localized surface plasmon resonances arising from p-type carriers in vacancy-doped semiconductor quantum dots that should allow for plasmonic sensing and manipulation of solid-state processes in single nanocrystals," says Berkeley Lab director Paul Alivisatos, a nanochemistry authority who led this research. "Our doped semiconductor quantum dots also open up the possibility of strongly coupling photonic and electronic properties, with implications for light harvesting, nonlinear optics, and quantum information processing."

Alivisatos is the corresponding author of a paper in the journal Nature Materials titled "Localized surface plasmon resonances arising from free carriers in doped quantum dots." Co-authoring the paper were Joseph Luther and Prashant Jain, along with Trevor Ewers.

The term "plasmonics" describes a phenomenon in which the confinement of light in dimensions smaller than the wavelength of photons in free space make it possible to match the different length-scales associated with photonics and electronics in a single nanoscale device. Scientists believe that through plasmonics it should be possible to design computer chip interconnects that are able to move much larger amounts of data much faster than today's chips. It should also be possible to create microscope lenses that can resolve nanoscale objects with visible light, a new generation of highly efficient light-emitting diodes, and supersensitive chemical and biological detectors. There is even evidence that plasmonic materials can be used to bend light around an object, thereby rendering that object invisible.

The plasmonic phenomenon was discovered in nanostructures at the interfaces between a noble metal, such as gold or silver, and a dielectric, such as air or glass. Directing an electromagnetic field at such an interface generates electronic surface waves that roll through the conduction electrons on a metal, like ripples spreading across the surface of a pond that has been plunked with a stone. Just as the energy in an electromagnetic field is carried in a quantized particle-like unit called a photon, the energy in such an electronic surface wave is carried in a quantized particle-like unit called a plasmon. The key to plasmonic properties is when the oscillation frequency between the plasmons and the incident photons matches, a phenomenon known as localized surface plasmon resonance (LSPR). Conventional scientific wisdom has held that LSPRs require a metal nanostructure , where the conduction electrons are not strongly attached to individual atoms or molecules. This has proved not to be the case as Prashant Jain, a member of the Alivisatos research group and one of the lead authors of the Nature Materials paper, explains.

"Our study represents a paradigm shift from metal nanoplasmonics as we've shown that, in principle, any nanostructure can exhibit LSPRs so long as the interface has an appreciable number of free charge carriers, either electrons or holes," Jain says. "By demonstrating LSPRs in doped quantum dots, we've extended the range of candidate materials for plasmonics to include semiconductors, and we've also merged the field of plasmonic nanostructures, which exhibit tunable photonic properties, with the field of quantum dots, which exhibit tunable electronic properties."

Jain and his co-authors made their quantum dots from the semiconductor copper sulfide, a material that is known to support numerous copper-deficient stoichiometries. Initially, the copper sulfide nanocrystals were synthesized using a common hot injection method. While this yielded nanocrystals that were intrinsically self-doped with p-type charge carriers, there was no control over the amount of charge vacancies or carriers.

"We were able to overcome this limitation by using a room-temperature ion exchange method to synthesize the copper sulfide nanocrystals," Jain says. "This freezes the nanocrystals into a relatively vacancy-free state, which we can then dope in a controlled manner using common chemical oxidants."

By introducing enough free electrical charge carriers via dopants and vacancies, Jain and his colleagues were able to achieve LSPRs in the near-infrared range of the electromagnetic spectrum. The extension of plasmonics to include semiconductors as well as metals offers a number of significant advantages, as Jain explains.

"Unlike a metal, the concentration of free charge carriers in a semiconductor can be actively controlled by doping, temperature, and/or phase transitions," he says. "Therefore, the frequency and intensity of LSPRs in dopable quantum dots can be dynamically tuned. The LSPRs of a metal, on the other hand, once engineered through a choice of nanostructure parameters, such as shape and size, is permanently locked-in."

Jain envisions quantum dots as being integrated into a variety of future film and chip-based photonic devices that can be actively switched or controlled, and also being applied to such optical applications as in vivo imaging. In addition, the strong coupling that is possible between photonic and electronic modes in such doped quantum dots holds exciting potential for applications in solar photovoltaics and artificial photosynthesis

"In photovoltaic and artificial photosynthetic systems, light needs to be absorbed and channeled to generate energetic electrons and holes, which can then be used to make electricity or fuel," Jain says. "To be efficient, it is highly desirable that such systems exhibit an enhanced interaction of light with excitons. This is what a doped quantum dot with an LSPR mode could achieve."

The potential for strongly coupled electronic and photonic modes in doped quantum dots arises from the fact that semiconductor quantum dots allow for quantized electronic excitations (excitons), while LSPRs serve to strongly localize or confine light of specific frequencies within the quantum dot. The result is an enhanced exciton-light interaction. Since the LSPR frequency can be controlled by changing the doping level, and excitons can be tuned by quantum confinement, it should be possible to engineer doped quantum dots for harvesting the richest frequencies of light in the solar spectrum.

Quantum dot plasmonics also hold intriguing possibilities for future quantum communication and computation devices.

"The use of single photons, in the form of quantized plasmons, would allow quantum systems to send information at nearly the speed of light, compared with the electron speed and resistance in classical systems," Jain says. "Doped quantum dots by providing strongly coupled quantized excitons and LSPRs and within the same nanostructure could serve as a source of single plasmons."

Jain and others in Alivsatos' research group are now investigating the potential of doped quantum dots made from other semiconductors, such as copper selenide and germanium telluride, which also display tunable plasmonic or photonic resonances. Germanium telluride is of particular interest because it has phase change properties that are useful for memory storage devices.

"A long term goal is to generalize plasmonic phenomena to all doped quantum dots, whether heavily self-doped or extrinsically doped with relatively few impurities or vacancies," Jain says.

The Daily Californian Online

Scientists make advancements in field of plasmonics

By Kate Randle
Daily Cal Staff Writer
Thursday, April 21, 2011
Category: News > University > Research and Ideas

Amirpasha Moghtaderi/Staff
A new development was created through research in plasmonics.

In an age when technological grandeur is marked by the speed of a device, scientists at the Lawrence Berkeley National Laboratory have made an advancement in the field of plasmonics that would broaden the range of materials used to make, among other things, extremely fast computers.

Plasmonics is a field that studies the interaction of light with nanoscale structures. The research - published online April 10 in the journal Nature Materials - indicates that localized plasmonic surface resonances are not only displayed in metals but can also exist in semiconductor nanocrystals called quantum dots.

This means that the frequency of plasmonic resonances can be manipulated to improve the efficiency of the products in which they are used - such as computers.

According to Prashant Jain, a UC Berkeley postdoctoral researcher who co-authored the study, creating computers that run on plasmons rather than electrons - which is what current computers run on - would be impossible without the controllable frequencies characteristic of plasmonics in semiconductors. Such computers would be faster, as photons travel faster than electrons without losing energy through resistance.

"To create a photonic computer you need all these tiny photonic components," he said. "If you want one that's switchable you can't use a metal, but you can use a semiconductor because their interaction with light can switch on and off."

Yongmin Liu, a postdoctoral researcher in UC Berkeley's Department of Mechanical Engineering, said the relatively small wavelengths of plasma can focus light on small areas. This feature can be used to make patterns on computer chips that would increase density for information storage.

Co-author Joseph Luther, currently a senior research scientist at the National Renewable Energy Lab in Colorado, conducted postdoctoral research with Paul Alivisatos, a corresponding author and director of the Lawrence Berkeley National Laboratory, whose research group helped conduct studies at the lab.

Luther said the team wanted to see if plasmonic properties could arise in non-metallic materials, a theory that had not yet been proven. To do this, they tested the properties of the semiconductor copper-sulfide.

"Since the nanocrystals didn't have as much copper as did sulfur, they're what are called copper vacancies," he said. "When (a copper atom) is not there, you basically have a localized charge in that one vacancy. What we noticed was that they behaved like a metal that had a plasmon."

Four authors - including Jain - found that pure copper sulfide without those vacancies did not demonstrate the same plasmonic qualities.

According to Jain, by exposing the material to a chemical oxidant, researchers "doped" it, which made it an impure substance. This allows it to display plasmonic resonance.

Research has already been conducted on semi-conductors and plasmonic resonance. However, this is the first time plasmonics and semi-conductors have been merged into a single field.

"There were two communities of researchers," Jain said. "One was on nanostructures, photonics and plasmonics. The other was working on semiconductors, quantum dots and the whole nanoelectronics and computer fabrication industry. This paper basically combines research from both and makes a combined field of quantum dot plasmonics."

Tags: , Lawrence Berkeley National Lab, plasmonics

Article Link: http://www.dailycal.org/article/112884

Surface plasmon laser based on metal cavity array with two different modes

Jiaqi Li, [1, 2,†] Yuan Zhang, [1,†] Ting Mei,[3,*] and Michael Fiddy[4, 5]

[1]Nanophotonics Lab, School of Electrical and Electronic Engineering, Nanyang Technological University, 639798, Singapore.
[2]Physics Department, Southeast University, Nanjing 211189, China
[3]Institute of Optoelectronic Materials and Technology, South China Normal University, Guangzhou 510631, China
[4]Center for Optoelectronics and Optical Communications, University of North Carolina at Charlotte, Charlotte NC 28223, USA
[5]mafiddy@uncc.edu
[*]ting.mei@ieee.org
[†] These authors contributed equally to this work

Abstract: The phenomenon of surface plasmon (SP) laser based on a square array of rectangular cavities cut into a metal substrate has been investigated. Both main resonant modes of the proposed structure can be used to realize SP laser while the working mechanism is different. We study the origin of these differences and propose an efficient design that exploits them. Besides, the effect of the sample size on SPP mode lasing is also discussed.

©2010 Optical Society of America

OCIS codes: (250.5403) Plasmonics; (310.6628) Subwavelength structures, nanostructures.

References and links

1. D. J. Bergman, and M. I. Stockman, "Surface plasmon amplification by stimulated emission of radiation: quantum generation of coherent surface plasmons in nanosystems," Phys. Rev. Lett. **90**(2), 027402 (2003).
2. M. I. Stockman, "Spasers explained," Nat. Photonics **2**(6), 327–329 (2008).
3. J. A. Gordon, and R. W. Ziolkowski, "The design and simulated performance of a coated nano-particle laser" Opt. Expr. **15**, 2622 (2007), *http://www.opticsinfobase.org/oe/abstract.cfm?URI=oe-15-5-2622.*
4. M. Wegener, J. L. Garcia-Pomar, C. M. Soukoulis, N. Meinzer, M. Ruther, and S. Linden, "Toy model for plasmonic metamaterial resonances coupled to two-level system gain" Opt. Expr. **16**, 19785 (2008), *http://www.opticsinfobase.org/oe/abstract.cfm?URI=oe-16-24-19785.*
5. Z. G. Dong, H. Liu, T. Li, Z. H. Zhu, S. M. Wang, J. X. Cao, S. N. Zhu, and X. Zhang, "Resonance amplification of left-handed transmission at optical frequencies by stimulated emission of radiation in active metamaterials" Opt. Expr. **16**, 20974 (2008),*http://www.opticsinfobase.org/oe/abstract.cfm?URI=oe-16-25-20974.*
6. N. I. Zheludev, S. L. Prosvirnin, N. Papasimakis, and V. A. Fedotov, "Lasing spaser," Nat. Photonics **2**(6), 351–354 (2008).
7. Z. G. Dong, H. Liu, T. Li, Z. H. Zhu, S. M. Wang, J. X. Cao, S. N. Zhu, and X. Zhang, "Modeling the directed transmission and reflection enhancements of the lasing surface plasmon amplification by stimulated emission of radiation in active metamaterials," Phys. Rev. B **80**(23), 235116 (2009).
8. M. A. Noginov, G. Zhu, A. M. Belgrave, R. Bakker, V. M. Shalaev, E. E. Narimanov, S. Stout, E. Herz, T. Suteewong, and U. Wiesner, "Demonstration of a spaser-based nanolaser," Nature **460**(7259), 1110–1112 (2009).
9. M. Ambati, S. H. Nam, E. Ulin-Avila, D. A. Genov, G. Bartal, and X. Zhang, "Observation of stimulated emission of surface plasmon polaritons," Nano Lett. **8**(11), 3998–4001 (2008).
10. A. Banerjee, R. Li, and H. Grebel, "Surface plasmon lasers with quantum dots as gain media," Appl. Phys. Lett. **95**(25), 251106 (2009).
11. C. P. Huang, J. Q. Li, Q. J. Wang, X. G. Yin, and Y. Y. Zhu, "Light reflection from a metal surface with subwavelength cavities," Appl. Phys. Lett. **93**(8), 081917 (2008).
12. C. P. Huang, Q. J. Wang, and Y. Y. Zhu, "Dual effect of surface plasmons in light transmission through perforated metal films," Phys. Rev. B **75**(24), 245421 (2007).
13. C. F. Klingshirn, *Semiconductor Optics*, (3rd edition, Springer, 2007).
14. M. I. Stockman, "The Spaser as a nanoscale quantum generator and ultrafast amplifer," J. Opt. **12**(2), 024004 (2010).

1. Introduction

In the past ten years, advances in nanotechnology have stimulated the study of Surface Plasmon Polaritons (SPPs) which have importance in many new areas. One main consequence of SPPs is that electromagnetic (EM) fields can be strongly localized and enhanced at the metal and dielectric interface. When SPPs are generated, strong interactions will occur between the EM fields and the local material properties, which can be treated as an EM cavity. By combining SPPs with gain media, Bergman and Stockman introduced the new concept of a SPASER (Surface Plasmon Amplification by Stimulated Emission of Radiation) [1,2] suggesting a new kind of laser. Recently some simulations [1,3–7] and experiments [8–10] have appeared which show that the stimulated SPP could provide a very useful source in bio-sensing. One example of the proposed SPASER [4–7] is based on a metamaterial (i.e. a periodic array of sub-wavelength elements) which shows a strong field confinement at a resonant frequency. Unfortunately, fabrication has proved an obstacle realizing such a meta-structure for visible or infrared wavelengths. This is because the unit cell of the metamaterial needs dimensions of the order of a tenth of the wavelength being employed, requiring the size of the elements in each unit cell to be even smaller. In this paper, we propose a periodic array of cavities in a metal substrate which exhibits two resonant modes. With the appropriate design, both modes can provide good field confinement that can be used to realize the surface plasmon (SP) laser phenomenon, but the working principle is different between the two modes. At visible and infrared wavelengths, comparing our design with those based on metamaterials proposed by others, ours is simpler and more straightforward to make using existing fabrication technology.

2. The structures and its passive response

A cavity array under investigation is shown in Fig. 1. It comprises cuboid cavities, arranged in a square array with lattice constant p, which are carved into a semi-infinite metal substrate and the bottoms are closed. Each cavity has dimensions of a, b and t in the x, y and z directions, respectively. The metal substrate is covered by a dielectric layer with thickness h and the background material is air. For convenience, we define the dielectric cover-layer as region I and the cavities as region II. The permittivity of the metal, the medium in the cavities, the cover-layer, and the air are denoted by ε_m, ε_{II}, ε_I and ε_0, respectively and we adopt the Drude model to describe the metal permittivity. Linearly polarized light, with the electric field along the x direction, is incident normal to the metal surface and is reflected into the air.
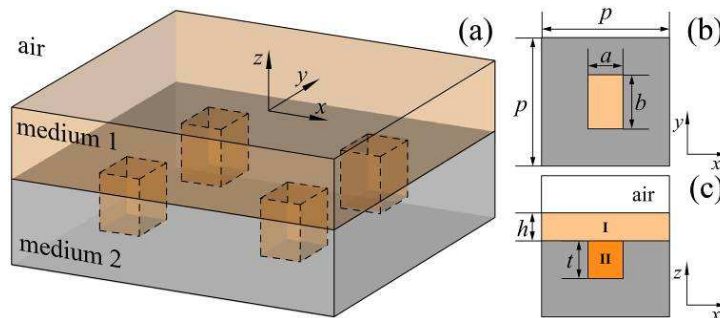

Fig. 1. (a) the schematic of our designed structure; a square array of cuboid cavities are carved into the metal substrate with a dielectric overlay, (b) the top-view and (c) the side-view of the unit cell, where p = 1100nm, a = 250nm, b = 375nm, t = 500nm, h = 250nm.

In order to understand the spectral response of this structure, a numerical simulation based on the full-wave finite element method was carried out. Parameters are set as: p = 1100nm, a = 250nm, b = 375nm, t = 500nm, h = 250nm, and $\varepsilon_I = \varepsilon_{II}$ = 2.25, which are optimized for a high Q cavity mode and a surface mode at communication wavelength (~1550nm). More

details of the geometry optimization can be found in Ref [11]. Besides, ε_m is silver having a Drude-type permittivity (ω_p = 1.37e16rad/s, γ = 8.85e13Hz), and background permittivity ε_0 = 1. The incident light has its electric field in x direction and magnetic field in y direction and we assume the ideal electric and magnetic boundary conditions are satisfied.
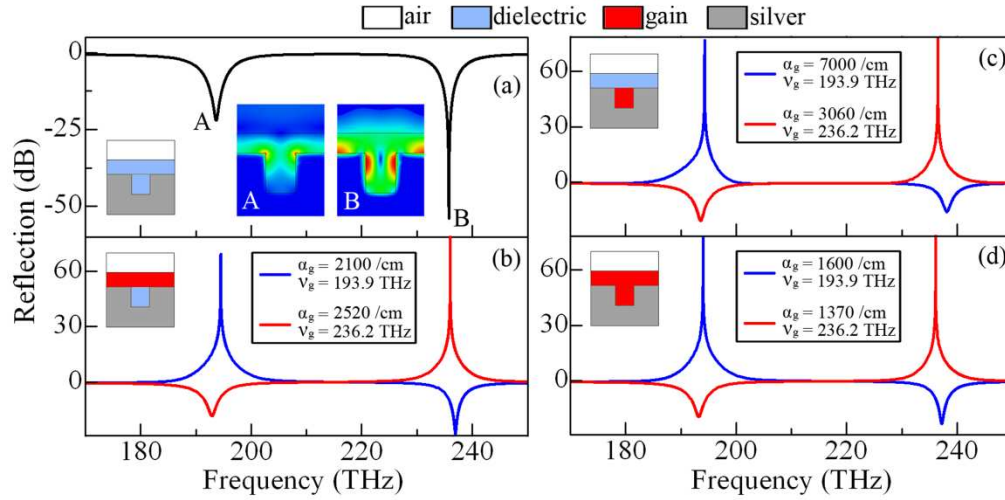

Fig. 2. The reflection spectra for normal incidence linearly polarized light on the periodic cavities for (a) the structure without gain media present and (b-d) the structure with gain media at different location as indicated in each inset. The red and blue curves represent the simulation results of gain media with different center frequencies at v_g = 193.9THz and v_g = 236.2THz, respectively. Inset A and B in (a) show the magnetic field (H_y) distribution corresponding dip A and dip B, respectively.

The spectrum of the reflected wave is shown in Fig. 2 (a) and indicates that there are two reflection minima at around 193.9THz (A) and 236.2THz (B), which means that strong absorption occurs around those frequencies. As shown, the absorption behavior in these two regions is quite different, since dip B is much sharper and deeper than dip A. To explain the origin of this difference, we have studied the magnetic field (H_y) distribution for the two cases. As illustrated in Fig. 2 (a), inset A and inset B are the corresponding H_y distributions to dip A and dip B, respectively. It is observed that the EM fields are localized in the metal substrate surface for both dips, but there is stronger EM field in the cavity for dip B. This is in agreement with Huang's result [11] that the field of an SPP mode is partly located in region I, and partly trapped into the cavity as a Cavity Surface Plasmon (CSP) mode. Thus dip A arises from the SPP mode and dip B originates from the coupling between the SPP and the CSP modes [12]. Compared to SPP mode, the CSP mode can induce more intense field localization in the cavity leading to a lower reflection minimum. The cut-off wavelength of the cavity is a key parameter here, which can be written as [11]:

$$\lambda_c = 2\pi\sqrt{\varepsilon_{11}/(u^2 + v^2)}, \tag{1}$$

where, u, v are determined by $u\tan(ua/2) = -ik_0\varepsilon_{11}/\sqrt{\varepsilon_m}$ and $v\tan(vb/2) = -ik_0\sqrt{\varepsilon_m}$, and k_0 is the wave vector in the free space. The wavelength of dip A (1546nm) is longer than the cut-off wavelength (1363nm), thus the CSP mode can't be excited and the SPP mode is the major contributor to the reflection minimum. In contrast, the SPP and CSP modes can exist simultaneously at the wavelength of dip B (1270nm, and its cutoff wavelength is 1426nm), and the CSP mode plays an important role as shown in the insets of Fig. 2 (a). Thus it can be seen that SPP mode and CSP mode play different roles in the reflection spectrum. Both modes can be used to realize an SP laser, but based on different principles, as discussed below.

3. SP laser based on different modes

The material in regions I and II can be chosen as gain media to realize SP laser. The CSP and SPP modes are surface modes, and the fields are confined to the groove dielectric/silver surface. The localized field has a strong interaction with the structure and if gain media are introduced, an efficient feedback mechanism is available. Because of the losses in the metal, there will be a threshold value of the gain media for the SP laser phenomenon. For our structure, because of the two different physical mechanisms that occur, the SPP field spreads over the surface while the CSP field is much more trapped inside the cavities and so at different locations in the gain medium, there will be different SP laser behavior.

To examine this, we set region I, region II and then region I + II to be gain media to study the effect of the location of regions of gain. The gain media considered here are dispersive, with permittivity described as [13]:

$$\varepsilon(\omega) = \varepsilon_b + \frac{\chi_0 \omega_g^2}{\omega_g^2 - \omega^2 + i\gamma_g \omega} \tag{2}$$

where ω is the angular frequency, ε_b is the background permittivity, ω_g is the resonant center angular frequency of the gain media, γ_g is the collision frequency representing the dissipation, and χ_0 is the coupling strength. For convenience, we defined the resonant frequency $\nu_g = \omega_g/2\pi$. The gain is described by the negative imaginary part of ε_b , similar to Ref [4–7], and thus the gain coefficient can be defined as:

$$\alpha = \frac{\omega}{100 \times c_0} \mathrm{Im} \sqrt{\varepsilon(\omega)} \tag{3}$$

Here, c_0 is velocity of light in vacuum, α has units of cm^{-1}, and α_g is defined as the highest value of α and $\alpha_g = \alpha(\omega_g)$.

In the following discussion, we set $\varepsilon_b = 2.25$. We note that ε_b just determines the optical path length of the wave in the gain media, thus for different ε_b we can obtain the same simulation results by adapting the geometry of the structure to get the same optical path length. Also, $\gamma_g = 1.26 \times 10^{14}$ rad/s means a full width at half maximum (FWHM) of the gain material emission peak of ~150nm, which is reasonable for materials working at infrared wavelengths, e.g., PbS quantum dots. To study the SP laser at the two different reflection dips, the resonant frequency ν_g is taken as 193.9 THz and 236.2 THz corresponding to dip A and dip B, respectively. The gain coefficient given in Fig. 2 (b), (c) and (d) are the optimized results, and the optimization process will be discussed in the content about Fig. 3 below.

First we consider only region I is filled with the gain medium (see inset in Fig. 2(b)), while the other parameters are the same as in Fig. 2 (a). For this situation, the SPP mode on the metal surface interacts with the gain medium and the CSP mode in cavities gives a negligible contribution to the SP laser. The result (see Fig. 2 (b)) shows that for dip A ($\nu_g = 193.9$ THz), high reflection peaks of more than 60 dB can be obtained when the gain coefficient is about $\alpha_g = 2100/cm$, which means that there is strong feedback and the stimulated emission of the SPP mode takes place. For dip B ($\nu_g = 236.2$ THz), to get a high enough (>60dB) reflection peak, the required gain coefficient is around $\alpha_g = 2520/cm$ which is higher than that of dip A. The reason for this is that the reflection corresponding to dip B originates from the coupling of the SPP and CSP modes as described earlier. Consequently the interaction between the surface field and the gain medium associated with dip B is weaker than that of dip A and there is a higher gain coefficient requirement for the SP laser effect at dip B.

Secondly, the location of the gain media in the structure is changed from region I to region II (see inset in Fig. 2 (c)). This means the CSP mode is the dominant factor for the interaction between the surface field and the gain medium. Intuitively, for the reflection dip A, there is little EM field interacting with the gain medium in the cavity because its wavelength is

beyond the cut-off wavelength of the cavity. In contrast, for dip B, the EM field enters the cavities leading to the CSP mode, and a high localized EM field inside the cavities. This deduction is confirmed by our simulations shown in Fig. 2 (c). Although, high reflection peaks can be realized for both dips, we note that the gain coefficient required for dip A is much higher (α_g is about 7000/cm) than that required for dip B (α_g = 3060/cm).

The final case is that both region I and region II are filled with the gain medium (see the inset in Fig. 2 (d)). This is a more efficient way to realize SP laser based on our structure since the SPP and CSP modes both contribute to the interaction between the surface EM field and the gain media. The calculated reflection curves are shown in Fig. 2 (d), and we can see that the gain coefficient can be quite low while still reaching a high reflection peak for both frequencies, as compared to those cases in Fig. 2 (b) and (c). We also notice that in Fig. 2 (d), the required gain coefficient is lower for dip B than that of dip A for the reasons given earlier. The EM field corresponding to dip B has longer interaction time and optical path in the gain medium and thus stronger feedback leading to better conditions for SP laser. This is also consistent with the reflection curves in Fig. 2 (a) which shows the reflection dip B is much deeper and sharper, i.e., higher Q factor for dip B than dip A. Q factor here is represented by the ratio of the center frequency and the FWHM of the resonance. The cavities are important for field localization and feedback when using the gain medium.
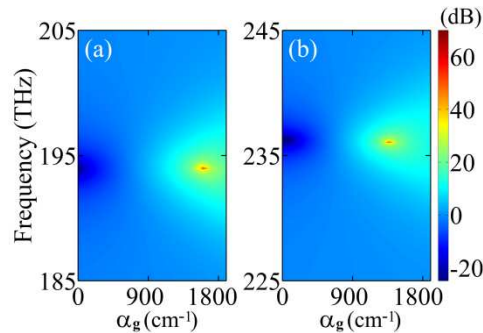

Fig. 3. (a) and (b) are calculated reflection spectra as function of α_g and frequency for dip A and dip B, respectively. Data are shown with a logarithm scale.

The SP laser reflection peaks in Fig. 2 are optimized results, that is, the peak does not continue to increase as the gain coefficient increasing. This effect in different SP laser designs has been studied and reported in Ref. 5 and 7. For the case of region I and II filled with gain media (as illustrated in Fig. 2 (d)), the relation of the reflection spectrum vs. gain coefficient has been calculated and shown in Fig. 3. The center frequency of the gain medium is still set to be ν_g = 193.9 THz for dip A and ν_g = 236.2 THz for dip B, and the maximum gain coefficient α_g is varied from 0 to 1800/cm. Initially, for both A and B, as the gain coefficient increases, the reflection amplitude increases to an optimum value (see those red areas in Fig. 3 (a) and (b)), and then begins to decrease if the gain coefficient keeps increasing further, which is similar to that reported in Ref. 5 and 7. In our simulation results, the width of resonance tends to be zero at the threshold of lasing and then broadens up again, owing to the fact that the gain medium is represented by an imaginary part of permittivity with negative value in this work, whereas the nature of the SP lasing as a spontaneous symmetry breaking, which leads to the establishment of the coherent SP state, is not considered [14]. Nevertheless, this simulation model is simple but useful for studying SP lasing before its lasing threshold [5–7].

The reflection peak corresponding to the SPP mode is caused by the surface periodicity, but factually, the sample should have a finite number of periods, which may limit the lasing. A sample with finite structure should be cut off along both x and y axis, but subject to the huge computational volume of a large 3D simulation, we study the problem for two separated cases, i.e. with cutoff along x and y directions respectively. The first has finite cell units in y

direction, denoted as $\infty \times n$, and the second has finite units in x, denoted as $m \times \infty$. As the electrical filed is always along x direction, implying that the surface plasmon oscillation is mainly along x axis, we can expect that the cutoff in x axis will have a dominant effect on lasing as confirmed by our simulation results. A small number of units in y direction is enough for lasing in the SPP mode. An example with n = 5 is shown in Fig. 4 (a) and (b)
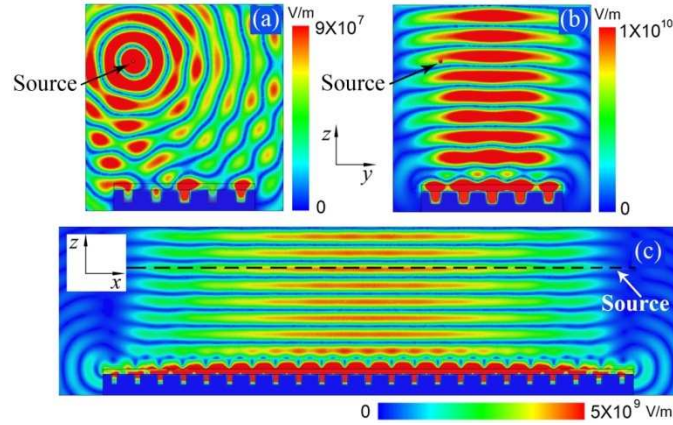

Fig. 4. Calculated E-field distribution for the SPP mode of finite array samples, (a) and (b) are corresponding to $\infty \times 5$ units array with and without gain medium, (c) $23 \times \infty$ units array with gain medium. The samples are illuminated by a line source along x-direction which are denoted by arrows.

without and with gain respectively. The calculation domain is 8um × 8um in y-z plane and one unit cell along x-direction. The two surfaces normal to x-direction are perfect electric boundaries and the other four surfaces are absorbing boundaries (such settings ensure we are simulating $\infty \times 5$ cells). The structure is illuminated by a line source (E-field along x direction), the field around the structure in (a) is nearly two orders of magnitude smaller than that in (b). Clearly, the source pattern in (b) has been covered by the lasing beam, compared to (a). When the cutoff occurs in x direction, more units along x are needed to get an output high enough. In Fig. 4 (c), the simulation result for the case m = 23 (i.e. $23 \times \infty$) is shown. The calculation domain is 30 um × 8 um in x-z plane, and one unit cell in y direction, the two surfaces normal to y-direction are perfect magnetic boundaries and the other four surfaces are absorbing boundaries (such settings ensure we are simulating $23 \times \infty$ cells). It is seen that the field becomes weaker towards the edges, because of periodicity breaking. This demonstrates that the amplified reflection can be realized by a sample with a finite number of periods and the sample edge scatter plays a limited adverse role.

4. Conclusion

The SP laser based on a cavity square array fabricated in a metal substrate has been studied. Both of the resonance modes of the structure can be used to realize the SP laser. By changing the gain media locations in the structure, results show that the CSP mode and SPP mode contribute quite differently when the SP laser is working at different resonant modes, which suggests that a joint contribution of CSP and SPP modes is the most efficient way to realize an SP laser. For SP laser of the SPP mode, the finite size could cause edge scattering and play negative role for lasing, but the influence can be improved when the sample contains enough units. Compared with those based on left-handed materials, this design is easier to implement using existing technology, and this work gives a new way to design an SP laser.

Simulation study of surface-plasmon-resonance electro-optic light modulator based on a polymer grating coupler

Wen-Kai Kuo* and Meng-Ting Chen

Department of Electro-Optics Engineering, National Formosa University, 64 Wenhua Road, Huwei, Yunlin, Taiwan 63208
*Corresponding author: wkkuo@nfu.edu.tw

An electro-optic light modulator design based on a grating-coupled surface-plasmon-resonance structure is numerically investigated using finite-difference time-domain simulation. The thickness effect of a dielectric layer acting as a waveguide on metal structures is investigated. The results show that the new structure has much higher modulation index than the conventional one and can implement an electro-optic modulator with low operating voltage. © 2009 Optical Society of America

OCIS codes: 240.6680, 050.2770, 230.4110.

A surface plasmon is an electromagnetic wave propagating along the surface of a metal and dielectric interface. Under phase-matching or resonance conditions, the energy of the incident light wave can be coupled to the collective oscillation of free electrons on the metal surface. This energy-transfer phenomenon can be achieved with p-polarized light by using either a prism or a grating coupler [1]. The energy transferred for excitation of the surface-plasmon resonance (SPR) is observed as a rapid decrease in reflectivity. Since the SPR is highly sensitive to changes in the refractive index on the metal surface, this technique has been extensively applied to biochemical sensing [2]; moreover, it has also played an important role in optical modulators. Further, the SPR technique can be combined with an electro-optic (EO) polymer in order to implement a simple and high-speed optical modulator. This type of device was theoretically described [3] and experimentally demonstrated later with different advancements [4–6]. Recently, a new type of a modulator that uses a resonant metal grating to greatly improve the modulation index has been proposed and numerically studied [7]. For the above modulators, prism coupling or the Kretschmann (KR) configuration is used for exciting SPR. However, this configuration requires a prism with high refractive index and therefore results in a noncompact and high-cost modulator.

A conventional grating coupler adapted for EO polymer modulation purpose and the reflectivity curves calculated as a function of the angle of incidence θ are shown in Fig. 1. This result is obtained by the EM Explorer, a 3D electromagnetic solver based on the finite-difference time-domain (FDTD) method [8]. In this structure as shown in the inset of the figure, a polymer layer with a thickness of 300 nm covers a gold grating with a modulation height of 70 nm and a pitch of 710 nm. The incident laser beam has a wavelength of 632.8 nm, and two polymer refractive indices are 1.489 and 1.490. The results reveal that the FWHM of the reflectivity curve exceeds 3°, and a nonsignificant resonance angle shift is observed on

increasing polymer refractive indices from 1.489 to 1.490. Hence, this structure can achieve only a very low modulation depth. A similar structure using a nanopolymer dispersed liquid-crystal EO material with high EO coefficients has been proposed [9]. Our new grating coupler structure is shown in Fig. 2. A similar structure has been previously described [10], and an implementation of such a structure has been demonstrated [11]. In [10], a grating structure is directly formed on a flat metal film; in [11], an elastomeric grating fabricated by the replica molding method is placed on the surface of a metal film. In the present study, the above structure is further modified by depositing a dielectric layer on the metal surface to function as a waveguide to improve the modulation index. A similar structure has been applied for excitation of the long-range SPR [12]; however, the thickness effect was not discussed. Through the thickness control, the new structure can be used to design an EO modulator with low operating voltage.
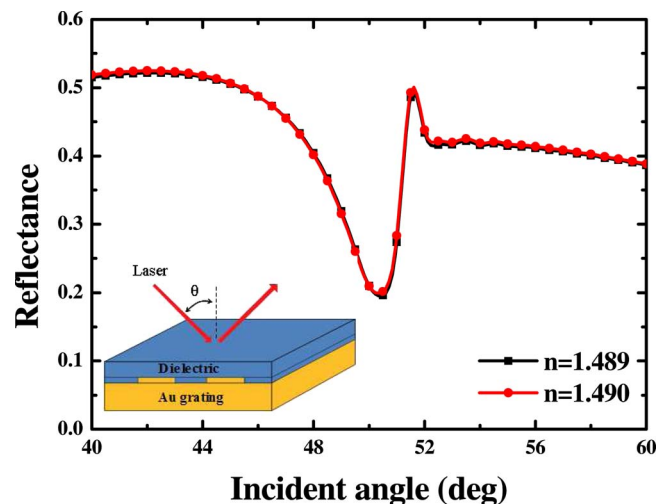

Fig. 1.   (Color online) Schematic of the SPR EO modulator based on a conventional grating coupler structure and reflectivity curves calculated as a function of the angle of incidence for two polymer refractive indices of 1.489 and 1.490.
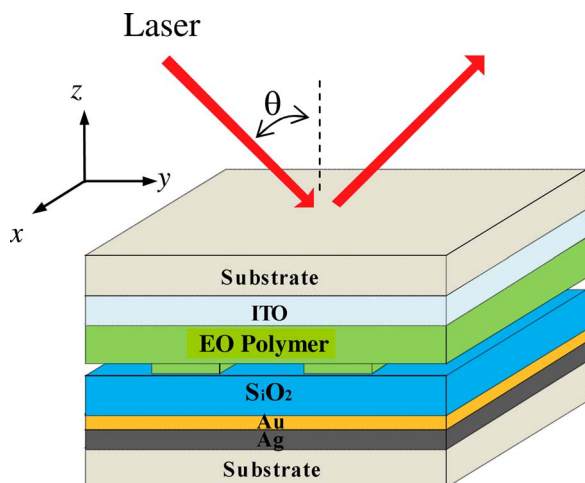
Fig. 2. (Color online) Schematic diagram of the grating coupler EO modulator with a passivation layer SiO_2 on Au. The thicknesses of silver, gold, SiO_2, polymer, and indium–tin–oxide (ITO) are 100 nm, 5 nm, 125 nm, 1 μm, and 100 nm, respectively. The modulation height and the pitch of grating structure are the same as those in Fig. 1.
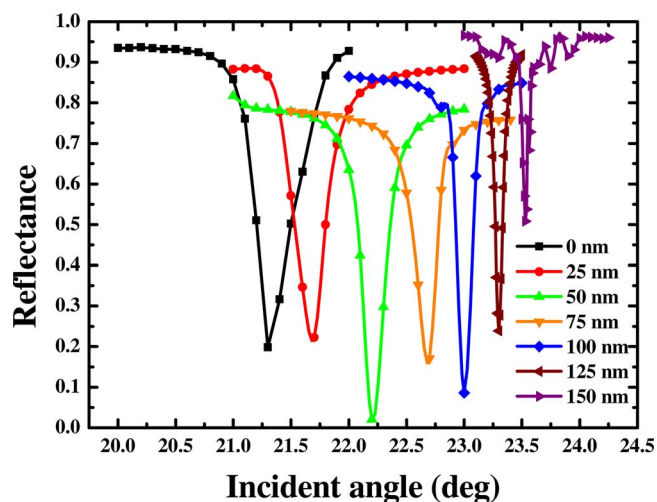

Fig. 3. (Color online) Reflectivity curves of the structure shown in Fig. 2 as a function of the angle of incidence for different thicknesses of the passivation dielectric layer from 0 nm to 150 nm in steps of 25 nm.

The new structure can be divided into two parts: the top glass substrate with an ITO layer and the grating structure on the downside, and the bottom glass substrate coated with dielectric, gold, and silver films on the upside. The refractive indices of all materials in this structure for simulation are as follows (from bottom to top): $n_0 = 1.515$ (glass), $n_1 = 0.14 + 4.15i$ (silver), $n_2 = 0.166 + 3.15i$ (gold), $n_3 = 1.457$ (dielectric passivation, SiO_2), $n_4 = 1.489$ (polymer), and $n_5 = 1.72$ (ITO). The thicknesses of silver, gold, SiO_2, polymer, and ITO are 100 nm, 5 nm, 125 nm, 1 μm, and 100 nm, respectively. The thicknesses of silver and gold are following the suggestion in [10]. The modulation height and pitch of the grating structure are the same as those in Fig. 1. In contrast to a high-refractive-index prism in the KR configuration, a glass substrate with a low refractive index of 1.515 is used here. Figure 3 presents calculated reflectivity curves by the EM explorer as a function of the angle of incidence for different thicknesses of the dielectric layer from 0 nm to 150 nm in steps of 25 nm. Because of the waveguide effect, the structures with a dielectric layer have a narrower FWHM than that without this layer. As the thickness of the dielectric layer increases, the propagation loss of the coupling wave in this grating-waveguide structure decreases and the quality factor increases, and hence the resonance width or the FWHM of the reflectivity becomes narrower. However, a too-thick dielectric layer decreases the energy transformation for excitation of the SPR and results in a high reflectivity at the resonance angle.

We choose the structure with a 125-nm-thick dielectric layer for further investigating, since this case has the narrowest resonance and still maintains a high plasmon-coupling efficiency of about 80%. For the gold-thickness effect, different gold thickness of 0 nm, 5 nm, and 10 nm for the case of 125-nm-thick dielectric layer are simulated, and the results show that the 5-nm-thick one gives the highest coupling ef-

ficiency and that the SPR FWHM is about 0.06°. For the structures with a 125-nm-thick dielectric layer and a 5-nm-thick gold film, two simulation curves with different EO polymer indices of 1.489 and 1.490 are shown in Fig. 4. As compared with Fig. 1, a significant resonance angle shift is observed when the same small increment is made in the refractive index of the polymer layer. For the EO polymer layer, if the poling field is applied along the z axis as the reference principal axes as shown in Fig. 3, after the poling process, the index ellipsoid of the poled polymer in the presence of a modulation electrical field $\mathbf{E} = (E_x, E_y, E_z)$ becomes [13]

$$\left(\frac{1}{n_o^2} + r_{13}E_z\right)(x^2 + y^2) + \left(\frac{1}{n_e^2} + r_{33}E_z\right)z^2 + 2r_{13}E_y yz$$
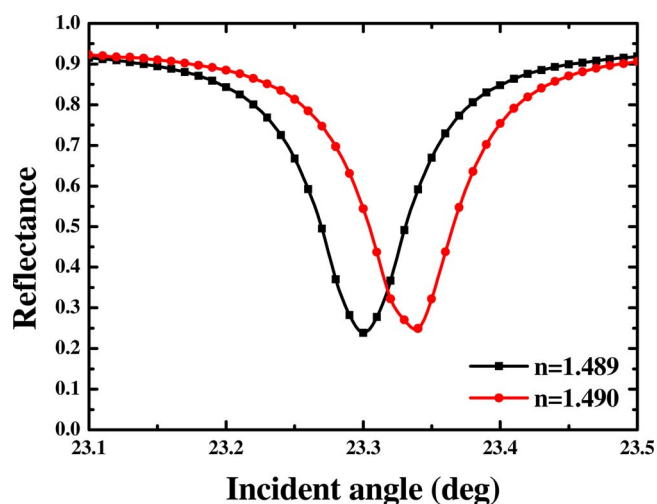$$+ 2r_{13}E_x xz = 1, \qquad (1)$$

Fig. 4. (Color online) Reflectivity curves of the structure shown in Fig. 2 with different EO polymer indices of 1.489 and 1.490. In this calculation, the thicknesses of dielectric layer and gold film are 125 nm and 5 nm, respectively.

where n_o and n_e are refractive indices of the poled polymer for ordinary and extraordinary rays, respectively, and r_{13} and r_{33} are the EO tensor elements. If the optical wave propagates along the y direction and only the z-axis electric-field E_z is applied, the index ellipsoid in Eq. (1) can be simplified as an index ellipse equation as

$$\left(\frac{1}{n_o^2} + r_{13}E_z\right)x^2 + \left(\frac{1}{n_e^2} + r_{33}E_z\right)z^2 = 1. \qquad (2)$$

For the optical wave to excite the SPR, its polarization direction is along z axis, and hence the corresponding refractive index change Δn of the EO polymer induced by the voltage V applied across the polymer is

$$\Delta n = \frac{1}{2}n_e^3 r_{33}\frac{V}{d}, \qquad (3)$$

where d is the thickness of the EO polymer and V/d corresponds to the electric-field E_z. Assuming that a polymer material with a high EO coefficient r_{33} of 200 pm/V is used and the incident angle θ is 23.28°, the reflectance as function of an applied voltage V is shown in Fig. 5. If the reflectivity bias point is set to 50%, a modulation index of 0.5 can be achieved by a low operating voltage of 2.5 V. Since this new structure is based on grating-coupled principle, the modulator operation is dependent on wavelength of the in-

cident light. Meanwhile, the modulator is a free-space type, the incident beam alignment accuracy should be controlled to better than 0.01° to obtain the expected performance. Regarding the device fabrication, the different structures located on two substrates can be fabricated separately and then assembled together by using adhering or bonding technique. The EO polymer grating structure can be fabricated by using simultaneous embossing and poling method [14].

In conclusion, a new structure of a grating-coupled SPR EO modulator with good modulation performance has been numerically demonstrated using the FDTD simulation. The resonance angle of this new configuration shifts significantly for a small-index increment of 0.001 in the EO polymer grating structure, and an EO modulator with low operating voltage can be achieved.
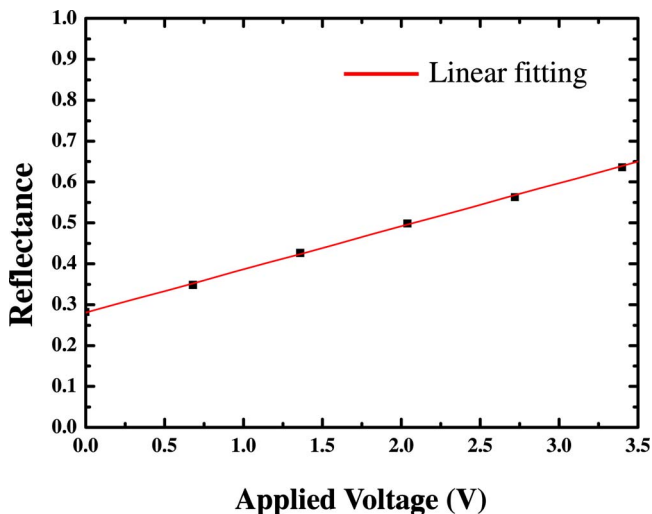
Fig. 5.   (Color online) Reflectance for a fixed incident angle with increasing applied voltage between the metal and ITO layers of the structure in Fig. 2.

References

1. H. Raether, *Surface Plasmons on Smooth and Rough Surfaces and on Gratings* (Springer-Verlag, 1988).
2. J. Homola, S. S. Yee, and G. Gauglitz, Sens. Actuators B **56**, 3 (1999).
3. J. S. Schildkraut, Appl. Opt. **27**, 4587 (1988).
4. O. Solgaard, F. Ho, J. I. Thackara, and D. M. Bloom, Appl. Phys. Lett. **61**, 2500 (1992).
5. C. Jung, S. Yee, and K. Kuhn, Appl. Opt. **34**, 946 (1995).
6. X. Deng, X. Zheng, Z. Cao, Q. Shen, and H. Li, Appl. Phys. Lett. **90**, 151124 (2007).
7. Z. Wu, R. L. Nelson, J. W. Haus, and Q. Zhan, Opt. Lett. **33**, 55 (2008).
8. A. Taflove and S. C. Hagness, *Computational Electrodynamics: the Finite-Difference Time-Domain Method*, 3rd ed. (Artech House, 2005).
9. S. Massenot, R. Chevallier, J.-L. de Bougrenet de la Tocnaye, and O. Parriaux, Opt. Commun. **275**, 318 (2007).
10. K. G. Muller, M. Veith, S. Mittler-Neher, and W. Knoll, J. Appl. Phys. **82**, 4172 (1997).
11. A. Kocabas, A. Dana, and A. Aydinli, Appl. Phys. Lett. **89**, 041123 (2006).
12. S. Glasberg, A. Sharon, D. Rosenblatt, and A. A. Friesem, Appl. Phys. Lett. **70**, 1210 (1997).
13. A. Yariv and P. Yeh, *Optical Waves in Crystals* (Wiley, 1983).
14. O. Sugihara, M. Nakanishi, H. Fujimura, C. Egami, and N. Okamoto, Opt. Lett. **25**, 1028 (2000).

Surface Plasmon Enhanced Light-Emitting Diode

Jelena Vučković, Marko Lončar, and Axel Scherer

Abstract—A method for enhancing the emission properties of light-emitting diodes, by coupling to surface plasmons, is analyzed both theoretically and experimentally. The analyzed structure consists of a semiconductor emitter layer thinner than $\lambda/2$ sandwiched between two metal films. If a periodic pattern is defined in the top semitransparent metal layer by lithography, it is possible to efficiently couple out the light emitted from the semiconductor and to simultaneously enhance the spontaneous emission rate. For the analyzed designs, we theoretically estimate extraction efficiencies as high as 37% and Purcell factors of up to 4.5. We have experimentally measured photoluminescence intensities of up to 46 times higher in fabricated structures compared to unprocessed wafers. The increased light emission is due to an increase in the efficiency and an increase in the pumping intensity resulting from trapping of pump photons within the microcavity.

Index Terms—Finite-difference time-domain methods, light-emitting diodes, optics at surfaces, spontaneous emission, surface plasmons.

I. INTRODUCTION

FOR years, a significant amount of scientific work has been focused on ways of improving the extraction efficiency of light-emitting diodes (LEDs). Many interesting approaches have been proposed to accomplish this, such as the use of thin light-emitting layers with surface texturing [1], resonant cavities [2], photon recycling [3], or output coupling through surface plasmons excited at corrugated metal surfaces [4]. External quantum efficiencies of 31% were reported by employing reflection from a bottom metal mirror together with a textured top semiconductor surface [5].

Apart from efforts to extract as much light as possible from a semiconductor device, it is also possible to enhance the light emission rate within a semiconductor. This approach is based on Purcell's prediction in 1946 that the radiation rate of an atom placed within a wavelength-sized cavity can be changed [6]. A fivefold enhancement of spontaneous emission was recently measured in a semiconductor optical microcavity at low temperatures [7], and Yablonovitch and coworkers demonstrated [8] that Purcell factors of about 55 can be achieved when a InGaN/GaN quantum well (QW) is positioned close to a thin silver layer.

In order to build an ideal, highly efficient light-emitting diode (LED), it is desirable to improve the extraction efficiency and simultaneously enhance the spontaneous emission rate. A 15-fold emission intensity enhancement, with Purcell factor $F_p = 2$ was observed in 2-D periodic thin film photonic crystals [9]. On the

TABLE I
LAYERS OF THE GROWN WAFER

	layer	thickness [nm]
8	p-GaAs cap	10
7	p-$Al_xGa_{1-x}As$, $x < 0.3$	20
6	undoped GaAs	10
5	undoped $In_{0.2}Ga_{0.8}As$ QW	8
4	undoped GaAs	10
3	n-$Al_xGa_{1-x}As$, $x < 0.3$	20
2	n-GaAs cap	10
1	undoped AlAs (sacrificial layer)	100
0	undoped GaAs substrate	-

other hand, Barnes [10] recently discussed a potentially highly efficient LED consisting of a metal clad dielectric microcavity with periodic texturing of one of metal layers. He noted that coupling to surface plasmon modes could improve light emission properties of the device. Our work, presented in this paper, is the first experimental demonstration of this novel method for enhancing the light emission from LEDs.

In Section II of this article, we describe the procedure that we developed for fabricating metal clad semiconductor microcavities with periodic texturing of the top, semitransparent metal layer. In Section III, we present the theoretical analysis of their band structures, electromagnetic fields, external and extraction efficiencies, Purcell factors, as well as the calculated transmission of pump power through the top surface and the increase in the pumping intensity resulting from trapping of pump photons within the microcavity. Finally, in Section IV, we present and discuss results of photoluminescence (PL) measurements from fabricated structures.

II. FABRICATION

Design of the grown wafer is shown in Table I. Wafer was designed for fabrication of electrically pumped devices and p- and n-doped layers were included. Layers 2–8 form the membrane that will be lifted off and sandwiched between two metal layers. The total membrane thickness is approximately 90 nm. The emission from the InGaAs/GaAs QW is centered at 986 nm, which corresponds to conduction-to-heavy hole band transitions (C-HH). There is also a peak at 930 nm, corresponding to conduction-to-light hole band transitions (C-LH), which becomes more prominent at high pumping levels. C-HH transitions couple to electric fields polarized in the QW plane (x-z plane). On the other hand, C-LH transitions couple twice as strongly to electric fields with polarization perpendicular to the QW plane (y direction) than to those polarized in the QW plane [11]. In the classical spontaneous emission model, C-HH transitions are represented with parallel dipoles,
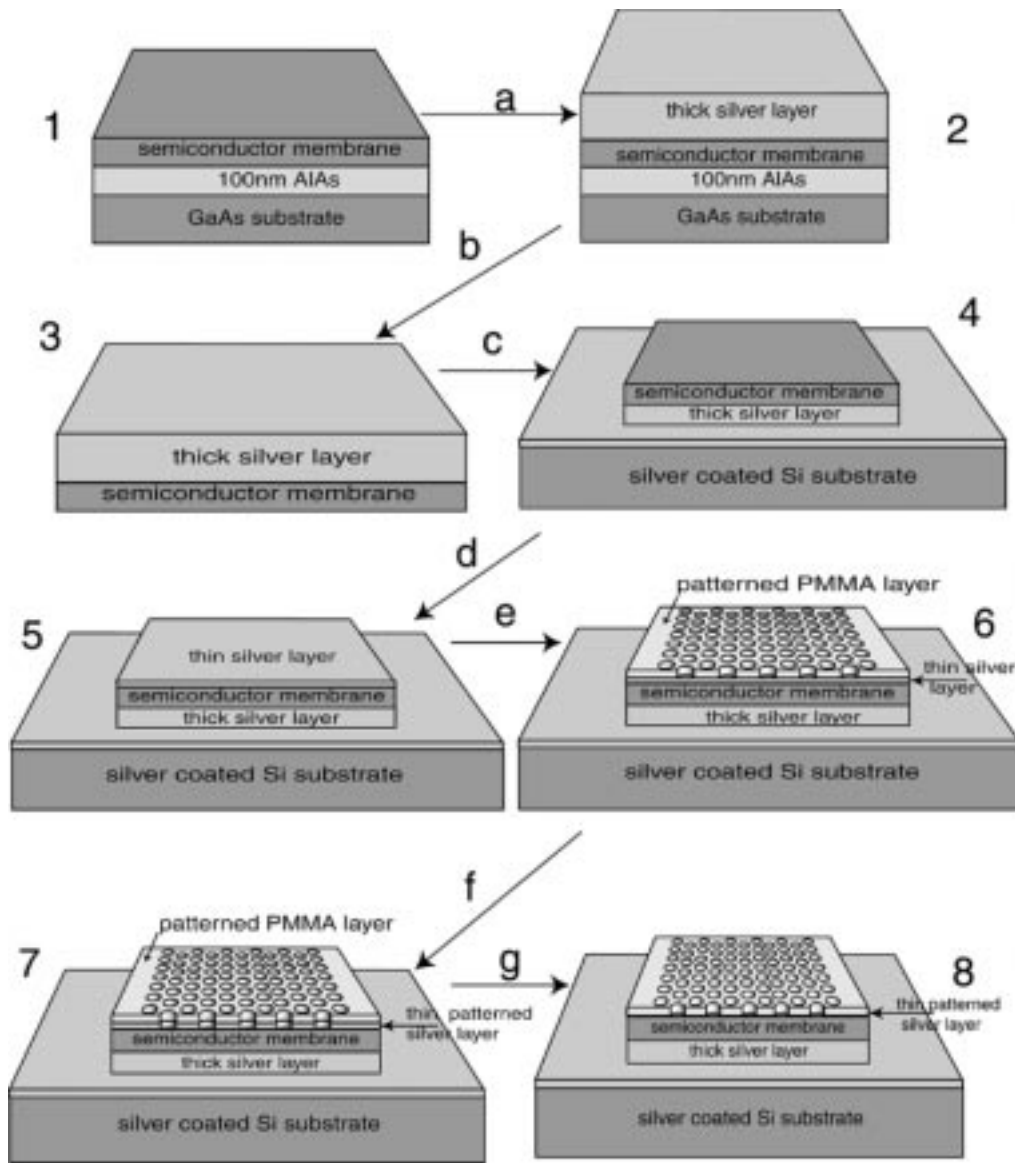
Fig. 1.   Fabrication procedure: (a) thick silver layer deposition; (b) epitaxial liftoff; (c) Van der Waals bonding onto silver coated silicon substrate; (d) thin silver layer deposition; (e) PMMA deposition and patterning using e-beam lithography; (f) pattern transfer to thin silver layer using Ar^+ ion milling; and (g) PMMA removal.

while C-LH transitions are represented with both parallel and perpendicular dipoles, weighted by factors of $1/3$ and $2/3$, respectively.

The fabrication procedure is described in Fig. 1. First, we deposit a thick silver mirror ($d > 1.5 \mu$m) on top of the grown wafer [step (a)]. This metal layer is also used as a mechanical support during the membrane liftoff. Then, we remove the membrane from its substrate by dissolving the sacrificial AlAs layer in 8.2% hydrofluoric acid (HF) diluted in water [step (b)]. HF attacks AlAs very selectively over $Al_xGa_{1-x}As$ for $x < 0.4$ [12]. The lifted-off membrane (layers 2–8) with the thick silver layer on top is then Van der Waals bonded [12] onto a silver coated silicon wafer and the silver on the lift-off film bonds to the silver coated on the silicon support wafer [step (c)]. Another 20–40-nm-thick silver layer is then deposited on top of the n-GaAs cap [step (d)]. A 100-nm-thick film of high molecular weight PMMA

(polymethylmethacrylate) is then spun on top of the thin metal layer and subsequently baked on a hot plate at 150 °C for 20 min. A desired pattern is beamwritten on the PMMA by electron beam lithography in a Hitachi S-4500 electron microscope [step (e)]. The resulting patterns are approximately 50 μm $\times$ 50 μm in size, and the exposed PMMA is developed in a 3:7 solution of 2-ethoxyethanol:methanol for 30 s. Then, the pattern is transferred into the top semitransparent metal layer using Ar^+ ion milling at a beam voltage of 1500 V [step (f)]. Finally, the remaining PMMA may be dissolved in acetone [step (g)]. A corresponding SEM picture, showing the top view of a fully processed wafer, is given in Fig. 2, where light areas correspond to regions where silver was removed.

The structure shown in Fig. 1.1 is the unprocessed wafer and the one in Fig. 1.4 is referred to as the half-processed wafer. Fig. 1.5 represents the unpatterned metal clad microcavity, and finally, the structure shown in Fig. 1.8 is the fully processed one.
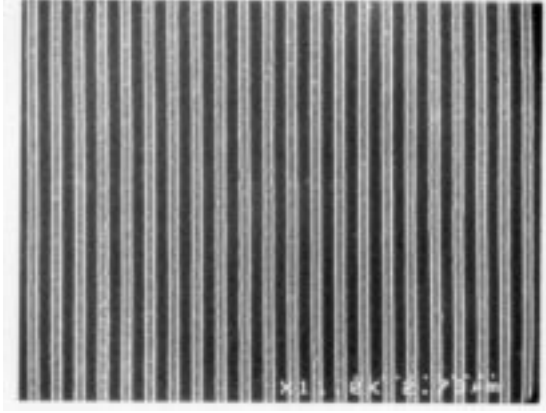
Fig. 2. Fabricated pattern in the top silver layer. Light areas correspond to regions where silver was removed during the Ar^+ ion milling process.

III. THEORY

A. FDTD Analysis of Metallic Structures at Optical Frequencies

The finite-difference time-domain (FDTD) method is used to theoretically analyze electromagnetic fields within metal clad microcavities. In order to accurately model metals at optical frequencies, it is necessary to make some changes [13], [14] to the standard Yee's FDTD scheme [15]. Electromagnetic fields in metals are described by adding a current term $(\vec{J})$ to Maxwell's curl equations (Drude model)

$$\vec{\nabla} \times \vec{H} = \epsilon_\infty \frac{\partial \vec{E}}{\partial t} + \vec{J} \tag{1}$$

$$\vec{\nabla} \times \vec{E} = -\mu_0 \frac{\partial \vec{H}}{\partial t} \tag{2}$$

$$\frac{\partial \vec{J}}{\partial t} + \nu \vec{J} = \epsilon_0 \omega_P^2 \vec{E} \tag{3}$$

where ω_p is the plasma frequency of a metal and ν is the corresponding damping rate. We assume that the metal is silver with parameters $\hbar\omega_p = 8.8$ eV (i.e., $\lambda_p = 140$ nm), $\hbar\nu = 0.05$ eV, and $\epsilon_\infty = \epsilon_0$. In part of our FDTD calculations, we neglect metal absorption losses by applying $\nu = 0$. Nonmetallic regions are described with standard Maxwell curl equations

$$\vec{\nabla} \times \vec{H} = \epsilon(\vec{r}) \frac{\partial \vec{E}}{\partial t} \tag{4}$$

$$\vec{\nabla} \times \vec{E} = -\mu_0 \frac{\partial \vec{H}}{\partial t}. \tag{5}$$

The FDTD method consists, basically, of the discretization of (1)–(5) in space and time [16]. The reader is referred to [17] for the detailed description of the FDTD calculation of band diagrams and filtering of electromagnetic fields for a mode of interest. Depending on the problem, different boundary conditions are applied to boundaries of the computational domain, such as the Mur's absorbing boundary conditions (Mur's ABC [18]) or Bloch boundary conditions. The spatial discretization step is critical in this case, keeping in mind that the penetration depth of the electromagnetic field into metals can be of the order of only tens of nanometers. This implies that large amounts of memory are required for computation unless variable cell sizes
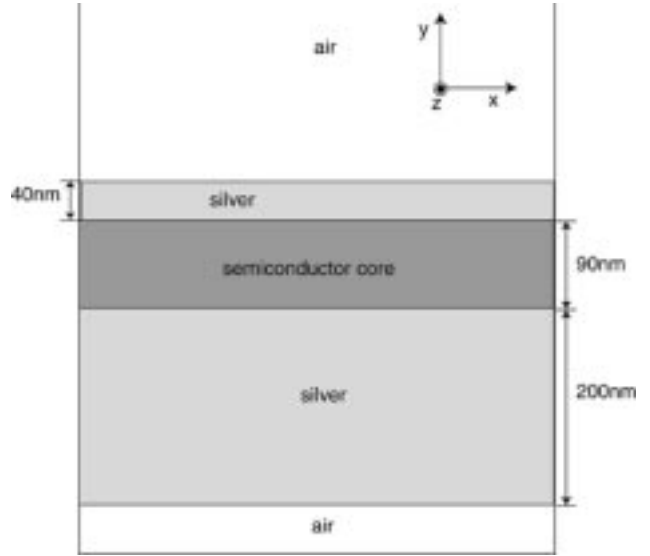

Fig. 3. A metal clad microcavity analyzed using the FDTD method. The structure is infinite in the z direction. Mur's absorbing boundary conditions are applied to boundaries in the y direction and Bloch boundary conditions are applied to boundaries in the x direction.

are used. We have performed 2-D analyses to design our structures, with discretization steps of 3 nm (unless noted otherwise).

B. Electromagnetic Fields and Band Diagrams of Unpatterned Metal Clad Microcavities

First, we analyze the band diagram of the metal clad microcavity shown in Fig. 3. Parameters of the analyzed structure are chosen so that they correspond to geometries which we have fabricated and measured. The semiconductor membrane was 90 nm thick, with a refractive index of $n = 3.5$. The top semitransparent silver layer was 40 nm thick, and the bottom silver layer was 200 nm thick. Absorption losses in silver were not included in any of the band diagram calculations, since if the bands are too lossy, it is difficult to recover them from spectra obtained in FDTD analyses. In the wavelength range of our interest (986 nm), the imaginary part of the silver dielectric constant is still much smaller than its real part, and positions of bands can be determined approximately by assuming that $\nu = 0$. The analyzed structure is surrounded by air on top and bottom and the slab is infinite in the horizontal plane. We assume that the structure is "periodic" in the x direction with an artificial periodicity of 50 nm and analyze only one unit cell. Mur's ABC are applied to boundaries in the y direction, while Bloch boundary conditions are applied to boundaries in the x direction.

P-polarized (TM) light has x and y components of the electric field and the z component of the magnetic field, while s-polarized (TE) light has x and y components of the magnetic field and the z component of electric field. The band diagram for the structure shown in Fig. 3 is shown in Fig. 4. The discretization step used in the FDTD calculation is equal to 1 nm. We observed that the increase in the discretization step (to 3 nm) influenced only the TM_0 band: the band shifted upwards in frequency at large k_x values. The splitting between the long- and short-range coupled SPP branches [10] of the top silver layer
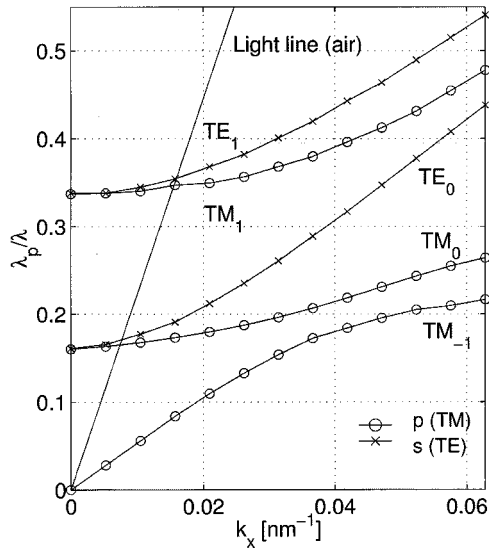
Fig. 4. Band diagram of the unpatterned (flat) metal clad microcavity. Silver layers are 40 and 200 nm thick and the semiconductor core thickness is 90 nm. Absorption losses in silver were not included.

Fig. 5. Intensities of electric and magnetic field components for the TM_{-1} mode, with $\lambda_p/\lambda = 0.084$ and $k_x = 0.0157$ nm^{-1}. The analyzed structure has the same parameters as the one whose band diagram is shown in Fig. 4.

was not observed for the semitransparent silver layer thickness used in FDTD calculations (40 nm) and for the used frequency resolution of $2.3 \cdot 10^{-3} \lambda_p/\lambda$. Let us analyze electromagnetic fields in the middle of the membrane, where the QW is located in real structures. The TM_{-1} mode has a very weak parallel (E_x) and a strong perpendicular (E_y) electric field component there, as shown in Fig. 5. It follows that perpendicular dipoles positioned in the QW couple strongly to this mode. On the other hand, the TM_0 mode has a strong parallel (E_x) and a weak perpendicular (E_y) electric field component in the middle of the membrane, as can be seen in Fig. 6. (Fig. 6 represents the TM_0 mode at cutoff where it is degenerate to the TE_0 mode and the y component of its electric field is equal to zero.) Furthermore, the TE_0 mode has only its parallel (E_z) component of electric field not equal to zero. Therefore, parallel dipoles in the QW couple strongly to TM_0 and TE_0 modes.

Using the 1-D finite difference method, we evaluated the cutoff frequency of TE_0 and TM_0 modes when absorption losses in both metal and semiconductor were included, and concluded that it was positioned at $\lambda_p/\lambda = 0.15$ instead of 0.16, as in the lossless band diagram shown in Fig. 4. Absorption losses also reduce the quality factors of modes. Using the FDTD method, we evaluated Q-factors corresponding to several $(k_x, \lambda_p/\lambda)$ points in the band diagram (including metal absorption) and they were in the range between 5–7. Therefore, for lossy bands, we cannot talk about an abrupt cutoff at $\lambda_p/\lambda = 0.15$. Instead, the cutoff is gradual and extends from about $\lambda_p/\lambda = 0.13$ to 0.15.

In normalized units, the C-HH transitions peak at 986 nm which corresponds to $\lambda_p/\lambda = 0.14$. From the previous discussion, it follows that these transitions couple mostly to TE_0 and TM_0 modes in the gradual cutoff. Their coupling to the TM_{-1} mode is very weak. On the other hand, the C-LH transitions peak at 930 nm corresponds to $\lambda_p/\lambda = 0.15$ and this emission couples strongly to the TM_{-1} mode. However, one third of C-LH
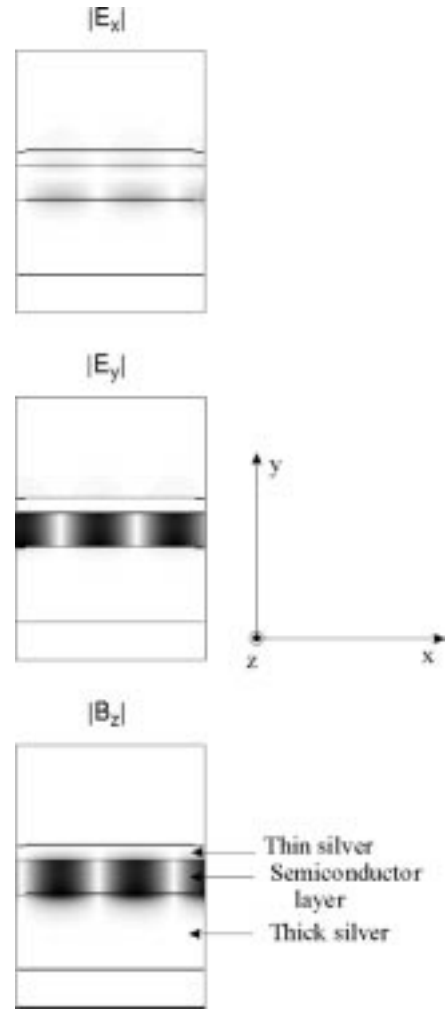
dipole transitions are in plane and they can couple to TE_0 and TM_0 modes.

C. Electromagnetic Fields and Band Diagrams of Metal Clad Microcavities with a Patterned Semitransparent Metal Layer

Perpendicular dipoles in metal clad microcavities couple strongly to the TM_{-1} mode [19] located below the light line, as shown in the band diagram in Fig. 4. Therefore, their emission cannot be extracted outside an unpatterned microcavity. Usually, the TM_{-1} mode is considered a loss mechanism in metallic structures. However, we can modify the band diagram and bring parts of the TM_{-1} branch above the light line by patterning of the top semitransparent metal layer. The introduction of periodicity into one of metallic layers dramatically changes the band diagram shown in Fig. 4. The band diagram is folded back into its first Brillouin zone at the edges of which the band gap for surface plasmon waves appears [10]. This means that bands previously located below the light line can now be brought above it. The effect of the periodic patterning can also be analyzed using the 2-D FDTD. We introduce a 1-D grating consisting of stripes (infinite in the
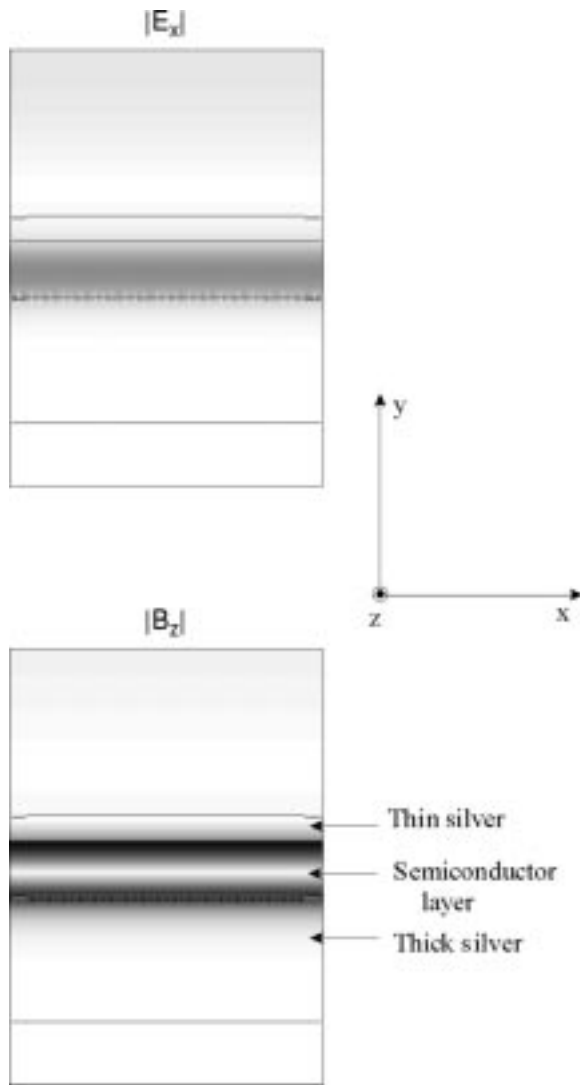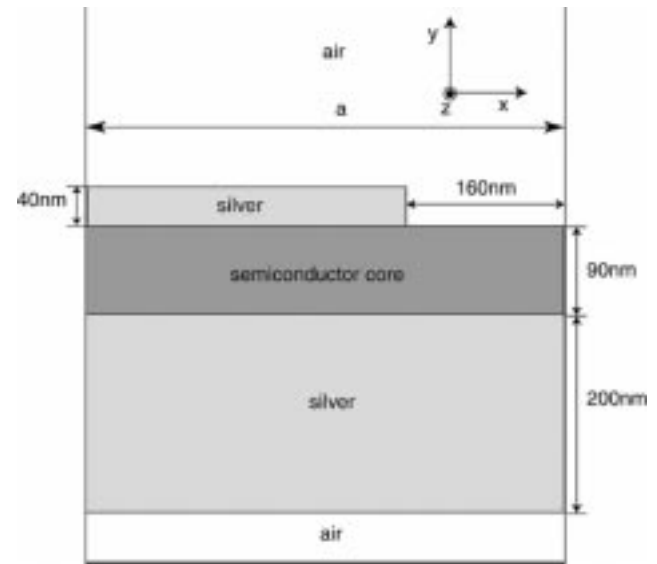
Fig. 7. The structure with a grating defined in the top semitransparent layer analyzed using the FDTD method in order to study the effect of metal patterning. Mur's absorbing boundary conditions are applied to boundaries in the y direction and Bloch boundary conditions are applied boundaries in the x direction. a denotes the grating periodicity.

Fig. 6. Intensities of the x component of the electric field and the z component of the magnetic field for the TM_0 mode, with $\lambda_p/\lambda = 0.16$ and $k_x = 0$. $E_y = 0$ for this mode. The analyzed structure has the same parameters as the one whose band diagram is shown in Fig. 4.

z direction) within the top metal layer. The pattern is formed by periodically modulating the top metal layer thickness between 40–0 nm. When the top layer is modulated between 20–0 nm, the results are approximately the same. We analyze three structures, with the same parameters as those that we fabricated and measured. Their grating periodicities are 250, 480, and 650 nm, with a 160-nm-wide gap between silver stripes. The schematic diagram of these structures is shown in Fig. 7 and the calculated band diagrams for TE and TM polarizations are shown in Figs. 8–10.

The indicator of how strongly the grating changes the band diagram of an unpatterned metal clad microcavity is the size of the band gap that opens at the edge of the Brillouin zone. Let us first consider band diagrams for the TM polarization. Clearly, in the frequency range of our interest $(\lambda_p/\lambda \cong 0.14)$ only the grating with a periodicity of 250 nm strongly affects properties of the structure. We expect that this grating will extract the emission of perpendicular dipoles, while the other two analyzed structures will not show any significant improvement over an unpatterned metal clad microcavity. With the frequency resolution of $2.3 \cdot 10^{-3} \lambda_p/\lambda$ used in our FDTD calculations, we could not detect a band gap at $k_x = 0$ and $\lambda_p/\lambda \cong 0.14$ for structures with periodicities of 650 or 480 nm. What about the TE polarization? A band with the cutoff frequency around 0.14 appears in TE band diagrams for all structures. As we will see from the electric field distribution, this branch corresponds to the combination of the TE_0 mode and the mode that resonates in the gap between silver stripes. For the smaller grating periodicity, gaps between silver stripes are closer to each other and behave as coupled cavities. Therefore, this mode can propagate in the x direction. On the other hand, for the larger grating periodicity (such as 480 nm), cavities are decoupled, this mode cannot propagate, and the corresponding TE band is flat. For the upper TE bands, the band gap does not appear at the edges of the Brillouin zone, meaning that the grating has basically no effect there and the corresponding mode is simply the TE mode of the unpatterned structure.

First, we filtered the TM polarized fields with $k_x = 0$ and $\lambda_p/\lambda \cong 0.14$ for the structure with a periodicity of 250 nm, in order to confirm that this metal layer patterning produces the outcoupling of radiation. From the band diagram shown in Fig. 8, we see that there are two modes in the filtered frequency range. The intensities of x and y components of electric field are shown in Fig. 11. By comparison with the fields from Fig. 5, we see that radiation now escapes from the microcavity, even though the gap between silver stripes is smaller than a wavelength. Moreover, the x component of the electric field is not negligible in the middle of the membrane. This means that parallel dipoles positioned there and oriented in the x direction can also couple to this mode. On the other hand, the E_y field is still strong within the membrane, which means that perpendicular dipoles still couple to this mode strongly.

Then, we filtered the TM polarized fields with $k_x = 0$ and $\lambda_p/\lambda \cong 0.15$, for the structure with a periodicity of 650 nm. The
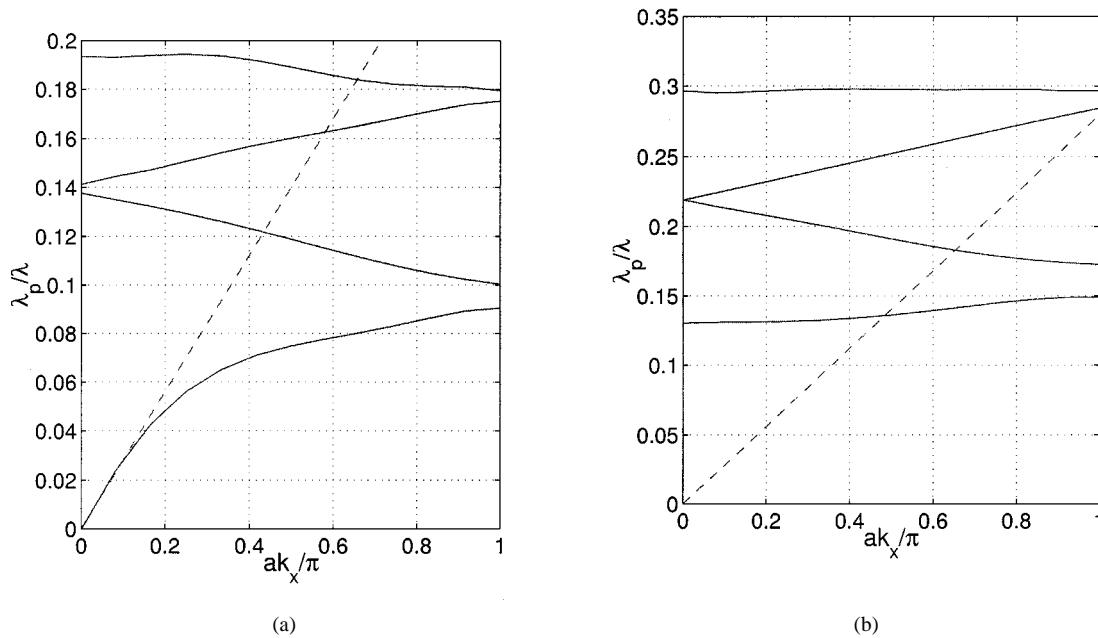
Fig. 8.   Band diagrams of the patterned structure with a periodicity of $a = 250$ nm: (a) TM-polarization and (b) TE-polarization. The dashed line corresponds to the light line in air.
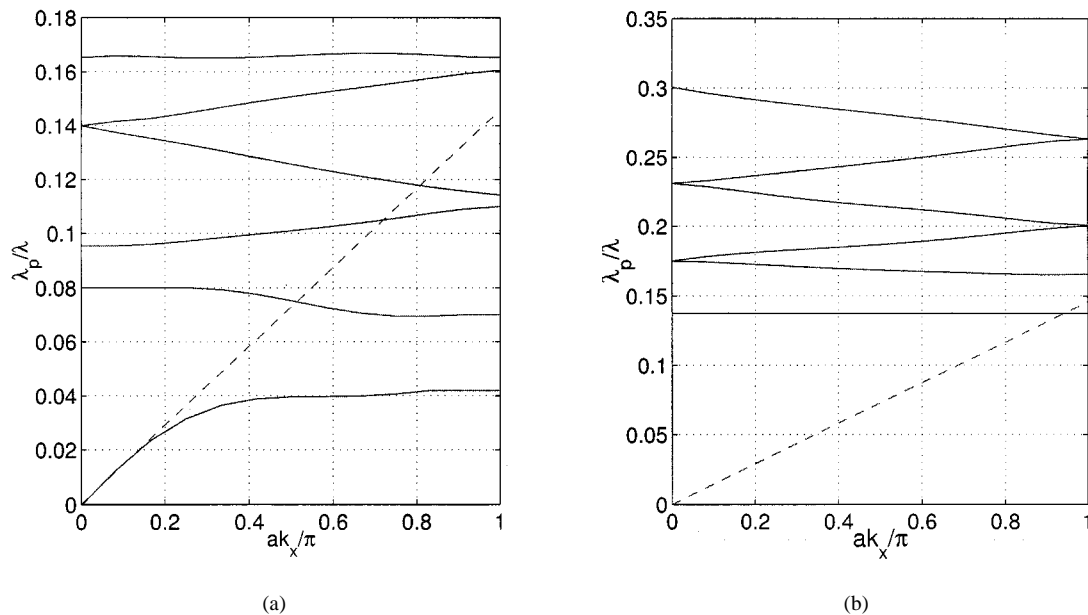

Fig. 9.   Band diagrams of the patterned structure with a periodicity of $a = 480$ nm: (a) TM-polarization and (b) TE-polarization. The dashed line corresponds to the light line in air.

electric field intensity patterns are represented in Fig. 12. They look exactly like the TM_{-1} mode with $k_x = 6\pi/a$ of the unpatterned structure, except underneath gaps between silver stripes. The electromagnetic field intensity outside the microcavity is small. This was expected from the band diagram for the TM polarization for this structure, shown in Fig. 10, since we could not detect opening of the band gap in the filtered frequency range.

We also filtered the TE polarized fields with $k_x = 0$ and $\lambda_p/\lambda \approx 0.14$ for the structures with periodicities of 250 and 480 nm. The corresponding E_z field distributions are shown in Fig. 13. The mode looks like the TE_0 mode that also resonates

in the gap between silver stripes, and is radiated out of the cavity through the spacing between stripes. Since the density of these spacings is larger for the structure with a periodicity of 250 nm, the mode will extract the emission out of this cavity more efficiently.

Therefore, the patterning of the top metal layer has a strong effect on properties of both TE and TM band diagrams. By choosing a grating appropriately, such as in the case of the analyzed structure with a periodicity of 250 nm, both the emission of perpendicular and parallel dipoles can be extracted out of the microcavity.
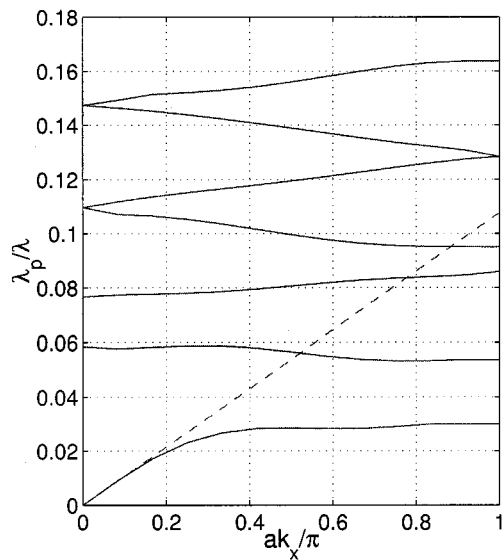
Fig. 10. Band diagram of the structure with a grating periodicity of 650 nm (TM-polarization only). The dashed line corresponds to the light line in air.

D. External Efficiency and Extraction Efficiency

Let us denote by $1/\tau_r$ the rate at which photons are radiated outside the cavity, and $1/\tau_{\mathrm{nr}}$ the decay rate corresponding to all other mechanisms (such as absorption losses or the excitation of modes that remain trapped within the cavity). The total decay rate is defined as

$$\frac{1}{\tau} = \frac{1}{\tau_r} + \frac{1}{\tau_{\mathrm{nr}}}. \tag{6}$$

The external efficiency (η_{ext}) can be expressed as [9]

$$\eta_{\mathrm{ext}} = \frac{\dfrac{1}{\tau_r}}{\dfrac{1}{\tau_r} + \dfrac{1}{\tau_{\mathrm{nr}}}} = \frac{\dfrac{1}{\tau_r}}{\dfrac{1}{\tau}}. \tag{7}$$

The external efficiency for planar structures without metal patterning can be evaluated using the method described in [20] and [21]. We calculated the external efficiency for the unpatterned metal clad microcavity with a 90-nm-thick semiconductor membrane, as a function of the top, semitransparent silver layer thickness, and for the collection angles of 30° or 90° with respect to the normal to the surface. The refractive index used for silver was $n = 0.14 + 6.94i$. The emitter was a parallel or a perpendicular dipole positioned in the middle of the membrane and oscillating at the wavelength of 986 or 930 nm. The calculated external efficiencies corresponding to perpendicular dipoles are negligible, while the external efficiencies of parallel dipoles are shown in Fig. 14. For the unprocessed wafer, we calculate that η_{ext} corresponding to parallel dipoles positioned 45 nm from the semiconductor/air interface is 2% into the 90° collection angle, or 0.5% into the 30° collection angle, both at wavelength of 986 and 930 nm. η_{ext} for perpendicular dipoles in the unprocessed wafer is negligible.
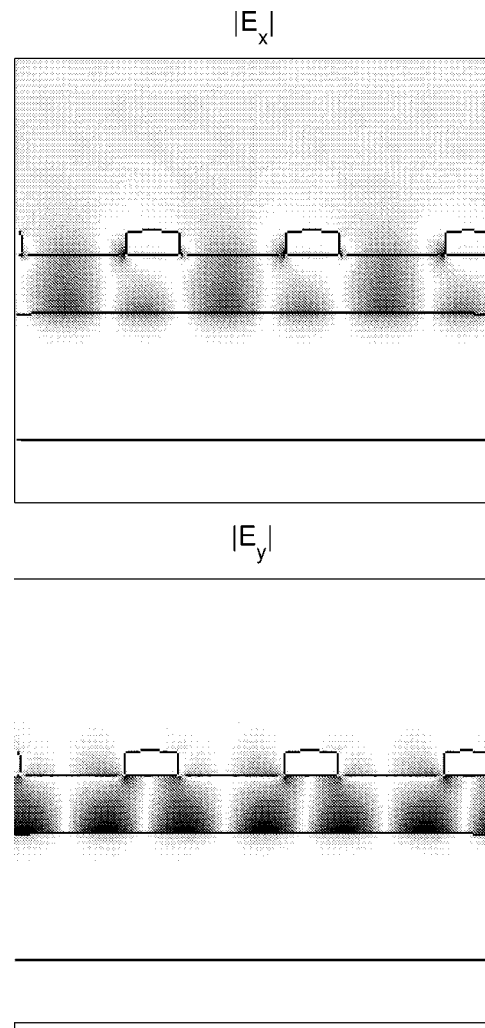

Fig. 11. Intensities of electric field components for the structure with a periodicity of 250 nm. The filtered frequency range was centered around $\lambda_p/\lambda = 0.14$ and $k_x = 0$.

For structures with a patterned top metal layer, external efficiencies can be calculated using the 3-D FDTD method, with oscillating dipole sources modeling atomic transitions. However, this computation would require large amounts of memory, as we noted previously. Instead, we can easily estimate, from our 2-D FDTD simulations, the efficiency of light extraction by coupling to some mode. The extraction efficiency η_x is the probability that a photon radiated into some mode escapes the cavity. The rate at which the electromagnetic field energy is lost from the cavity is described by the radiation quality factor Q_r.

$$Q_r = \frac{\omega_0 W}{P_r} \tag{8}$$

where W represents the electromagnetic field energy stored in the cavity, ω_0 is the radial frequency of a mode, and P_r is the power radiated outside the cavity. On the other hand, the nonradiative quality factor Q_{nr} describes the rate at which the stored electromagnetic energy decreases due to mechanisms other than the radiation outside the cavity

$$Q_{\mathrm{nr}} = \frac{\omega_0 W}{P_{\mathrm{nr}}} \tag{9}$$
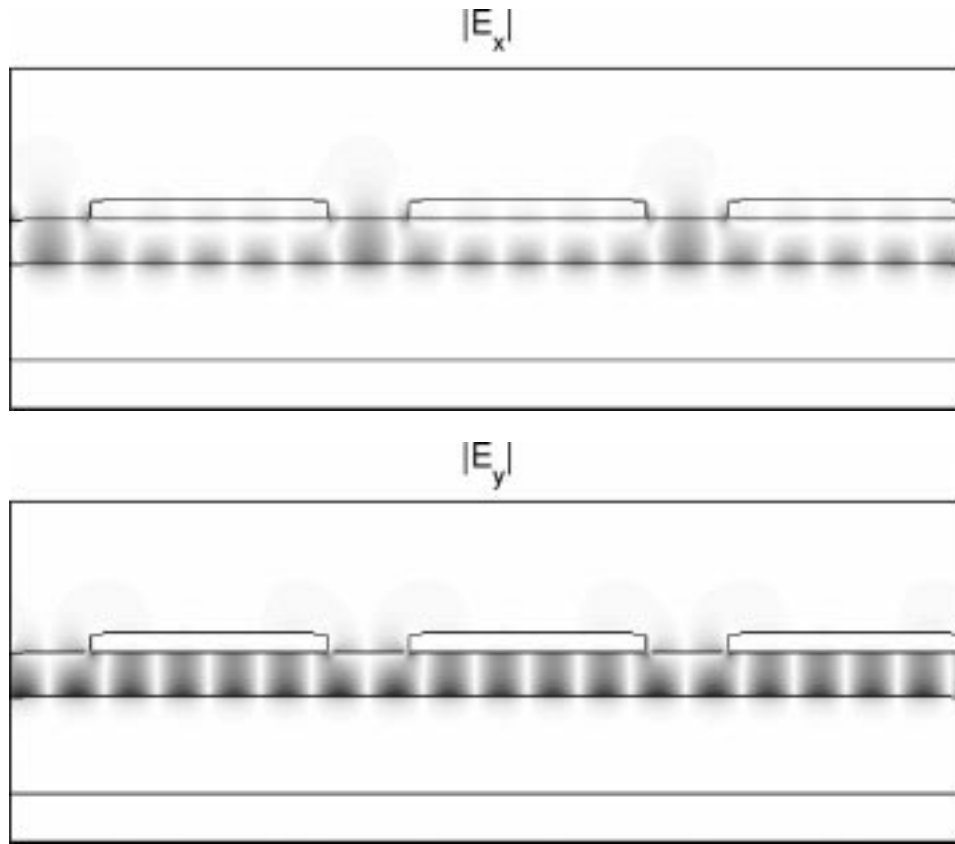
$$|E_x|$$

$$|E_y|$$

Fig. 12. Intensities of electric field components for the structure with a periodicity of 650 nm. The filtered frequency range was centered around $\lambda_p/\lambda = 0.15$ and $k_x = 0$.

where P_{nr} represents the power lost through these mechanisms. The total quality factor Q is defined as

$$\frac{1}{Q} = \frac{1}{Q_r} + \frac{1}{Q_{\mathrm{nr}}} \tag{10}$$

and the radiative and nonradiative photon lifetimes are defined as

$$\tau_{\mathrm{pr}} = \frac{Q_r}{\omega_0} \tag{11}$$

$$\tau_{\mathrm{pnr}} = \frac{Q_{\mathrm{nr}}}{\omega_0} \tag{12}$$

η_x can be expressed as

$$\eta_x = \frac{\dfrac{1}{\tau_{\mathrm{pr}}}}{\dfrac{1}{\tau_{\mathrm{pr}}} + \dfrac{1}{\tau_{\mathrm{pnr}}}} = \frac{Q}{Q_r}. \tag{13}$$

Clearly, η_x does not take into account the dependence on the position and orientation of dipole transitions, as well as all possible nonradiative mechanisms.

We calculated η_x for the structure with a periodicity of 250 nm. The only nonradiative loss mechanism in these calculations was the absorption in metal. For the folded TM$_{-1}$ mode, whose field distribution is shown in Fig. 11, we calculated Q_r between 30 and 50, $Q = 6$ and η_x between 12% and 20%. For the TE mode shown in Fig. 13, we calculated $Q_r = 15$, $Q = 5.5$ and $\eta_x = 37\%$. From the band diagram

shown in Fig. 8, we can see that the emission in the frequency range from 0.14 to 0.15 (in units of λ_p/λ) goes into the 30° escape cone, if coupled to TM modes. However, coupling to TE modes does not improve the directionality and the emission goes into the 90° cone. For the structures with periodicities of 650 or 480 nm, we estimated that $Q \cong 7$, while the extraction efficiencies corresponding to the folded TM$_{-1}$ branch were approximately the same as in the unpatterned cavity case. The calculated extraction efficiency corresponding to the first TE band (whose field distribution is shown in Fig. 13) in the structure with a periodicity of 480 nm is $\eta_x = 20\%$. However, only dipoles located directly underneath the gap between silver stripes can couple to this mode, which implies that the external efficiency is at least three times smaller than the calculated η_x. The situation is even worse in the structure with a periodicity of 650 nm. We conclude that the external efficiencies of the structures with periodicities of 480 and 650 nm are not expected to be better than in the unpatterned structure.

Therefore, for the structure with a periodicity of 250 nm, the extraction efficiency of more than 30% can be achieved in the presence of a grating. The filtered modes have low quality factors and overlap with both C-HH and C-LH emission peaks. From the field patterns for the TM mode shown in Fig. 11, we see that this mode can extract the emission of both perpendicular dipoles and parallel dipoles oriented in the x direction. On the other hand, the filtered TE mode extracts the emission of parallel dipoles oriented in the z direction. Since dipoles located in the middle of the membrane couple to these modes very strongly,
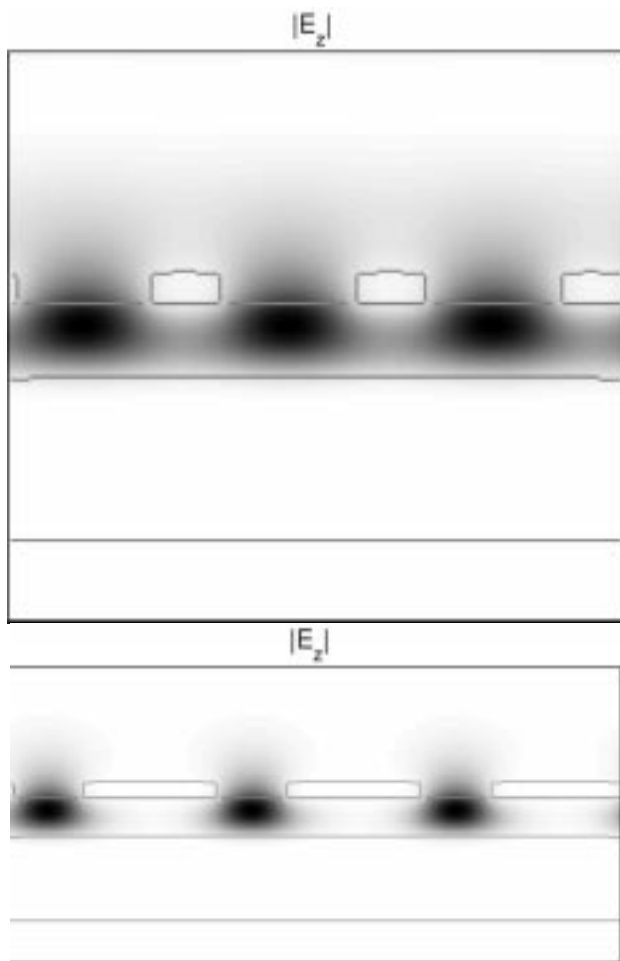
Fig. 13. $|E_z|$ of the TE mode with $k_x = 0$ and $\lambda_p/\lambda = 0.14$ for structures with periodicities of: (a) 250 and (b) 480 nm.
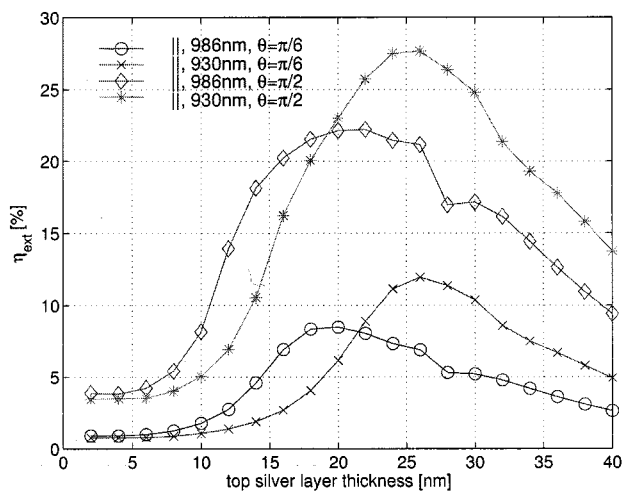

Fig. 14. Calculated external efficiency for the unpatterned metal clad microcavity, as a function of the top, semitransparent silver layer thickness. We calculated η_{ext} into the 30° or 90° collection angle. The emitter is a parallel dipole positioned in the middle of the 90-nm-thick membrane, oscillating at the wavelength of 986 or 930 nm.

we expect that this structure will have a better external efficiency than the unpatterned structure.
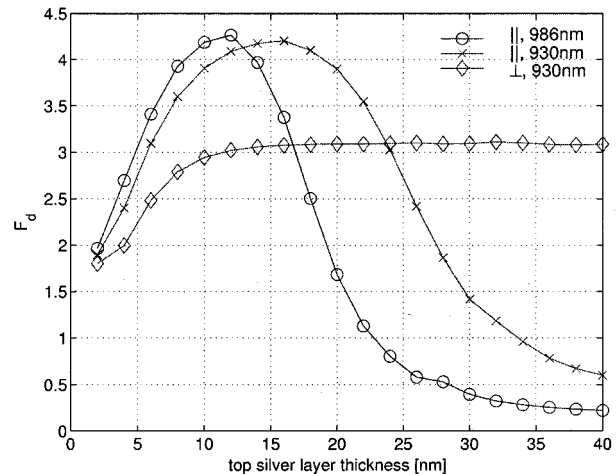

Fig. 15. Calculated decay rate enhancement for the unpatterned metal clad microcavity, as a function of the top, semitransparent silver layer thickness. The emitter is a parallel or a perpendicular dipole positioned in the middle of the 90-nm-thick membrane, oscillating at the wavelength of 986 or 930 nm.

One should also note low values of Q resulting from a significant metal absorption. A reduction in the absorption and a further increase in the extraction can be achieved by designing a device that operates at longer wavelengths. As we will see later, the calculated Q values are in the same range as our experimental results.

E. Purcell Factor and Decay Rate Enhancement

The Purcell factor (F_p) is defined as the spontaneous emission rate enhancement in a microcavity relative to a bulk semiconductor. On the other hand, we define the decay rate enhancement (F_d) as a ratio of the total decay rate in a microcavity $(1/\tau)$ and the spontaneous emission rate in a bulk semiconductor $(1/\tau_0)$

$$F_d = \frac{\dfrac{1}{\tau}}{\dfrac{1}{\tau_0}}. \tag{14}$$

The modulation speed of an LED is proportional to F_d. When analyzing a light-emitting device, we care about the overall efficiency, defined as a product of F_d and the external efficiency η_{ext}

$$F_d \cdot \eta_{\text{ext}} = \frac{\dfrac{1}{\tau_r}}{\dfrac{1}{\tau_0}}. \tag{15}$$

The efficiency is a measure of how much faster is the rate of light emission outside the cavity than the spontaneous emission rate in a bulk semiconductor.

We evaluated F_d analytically for unpatterned structures using the method described in [20]. The result is shown in Fig. 15. Subscripts $\|$ and $\perp$ denote parallel and perpendicular dipoles, respectively. If the excitation of surface plasmon modes is included in the spontaneous emission rate calculation
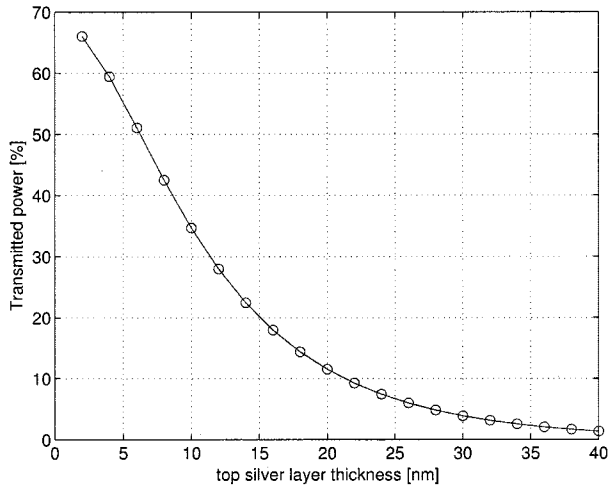
Fig. 16. Percentage of the pump beam intensity transmitted through the top, unpatterned silver layer, as function of its thickness.

for this structure, one obtains that $F_d \cong F_p$ for both parallel and perpendicular dipoles located in the middle of the membrane.

For complicated geometries obtained after the top metal layer patterning, it is possible to use the FDTD-based 3-D analysis of Purcell factor proposed in [22]. However, this requires large amounts of computer memory. Instead, it can be roughly assumed that decay rate enhancements and Purcell factors of fully processed, patterned structures have their values between those of the half-processed structure and the flat (unpatterned) metal clad microcavity.

F. Pump Power Transmission Through the Top Surface

In our experiments, we pump structures optically from top using a semiconductor laser diode emitting at 830 nm. Therefore, it is important to determine what percentage of the s-polarized pump beam is transmitted into the structure.

Let us denote by T the transmission through the top surface at the pump wavelength. T can be evaluated from Fresnel equations for an unpatterned top layer. The calculated T, as a function of the silver layer thickness, is shown in Fig. 16. The transmission through the air/semiconductor interface is equal to 70%. For structures with metallic grating on top, there is no increase in the pump power transmission due to diffraction at the patterned metal layer, and transmission coefficients can be approximated by weighting previously calculated coefficients with the filling factor of the grating. In order to prove that this is correct, we analyzed (using the 2-D FDTD method) the transmission through the metallic grating sitting on top of a semiconductor. The metal layer had the same parameters as the previously simulated grating with a periodicity of 250 nm and absorption losses were included. We analyzed one unit cell of the structure and applied Mur's ABC to boundaries in the y direction and periodic boundary conditions (i.e., Bloch boundary conditions with $k_x = 0$) to boundaries in the x direction. A parallel dipole (oriented in the x or z direction) was located 400 nm above the metal surface, in the air and above the middle of the gap between stripes. The frequency of dipole oscillations matched the pump frequency. We calculated the power of the dipole source,

as well as the power transmitted into the semiconductor, by integrating the Poynting's vector along a chosen surface. Without metal on top, the calculated transmission was $T = 0.7$ for both x-oriented or z-oriented dipole, as expected from Fresnel equations. However, in the presence of the metallic grating, we calculated $T = 0.5$ for an x-oriented dipole and $T = 0.24$ for a z-oriented dipole. This means that the average transmission in the presence of a grating is $T = 0.375$. By weighting transmission coefficients for the flat metal layer on top (40 nm thick) and for the air/semiconductor interface with the filling factor of the grating, we obtain $T = 0.47$.

G. Trapping of Pump Photons Within the Microcavity

We can define N as a factor that measures an increase in the pumping intensity resulting from the trapping of pump photons within the microcavity. N is proportional to an average number of times that a pump photon crosses the QW before being absorbed in it or lost through other nonradiative loss mechanisms. The trapping of pump photons within the microcavity effectively increases the pumping intensity, since the probability that a photon excites an electron transition into an upper band is proportional to the number of times that it crosses the QW. The unprocessed wafer has $N = 1$, since there is no mode within the structure that pump photons can couple to and photons not absorbed in the QW are lost when they reach the GaAs substrate. However, in the case of half-processed or fully processed wafers, the pump power transmitted through the top surface can couple to an s-polarized guided mode of the structure. For fully processed wafers, this can be easily seen from the previously calculated TE band diagrams (the pump wavelength is equal to 0.17 in units λ_p/λ). For the half-processed wafer, we performed the 1-D finite-difference analysis and showed that an s-polarized guided mode existed at the wavelength of 830 nm.

Let us denote by α (in units [1/cm]) the loss coefficient for the guided mode that pump photons couple to. The angle with respect to the y axis of this mode's total internal reflection is defined as

$$\theta = \arcsin\left(\frac{k_x}{k}\right) \qquad (16)$$

where k_x is the wavevector component in the direction of propagation (x) and k is the amplitude of the wavevector. Then, it follows that N is proportional to

$$N \cong \frac{1}{\alpha d \tan(\theta)} = \frac{\sqrt{k^2 - k_x^2}}{\alpha d k_x} \qquad (17)$$

where d is the membrane thickness. N cannot be considered to be the exact value of the increase in the pumping intensity, since we arbitrarily chose to evaluate it until the trapped beam energy drops to 10% of its initial value. However, it is the indicator that the trapping happens and how strong it is. We analyze the half-processed wafer and the flat metal clad microcavity using the 1-D finite difference method (absorption losses in both metal and semiconductor were included, former being dominant). From the obtained values of α and k_x for the guided TE mode at 830 nm, we estimate N. The unpatterned metal clad microcavity has $N = 12$, even when the top silver layer
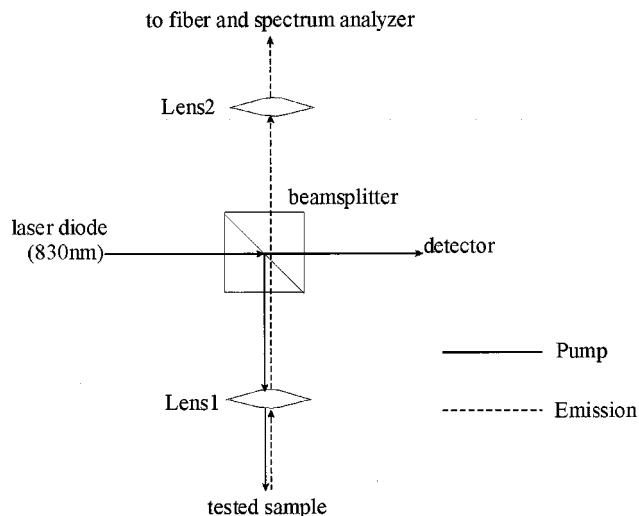
Fig. 17. Experimental setup used for PL measurements.

a [nm]	g [nm]	$E_{up}(986nm)$	$E_{hp}(986nm)$
250	160	46	2.24
480	160	5.6	-
650	160	6.4	-
0	0	5.5	-

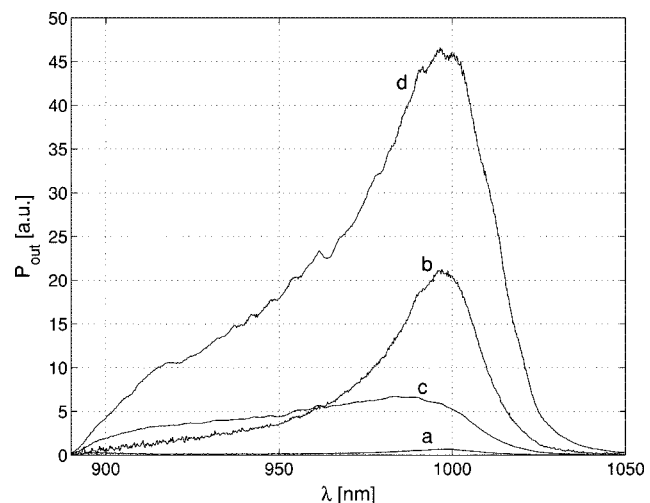Fig. 18. The measured PL spectra: (a) unprocessed wafer; (b) half-processed wafer; (c) pattern with $a = 650$ nm and $g = 160$ nm (the unpatterned structure and the pattern with $a = 480$ nm and $g = 160$ nm give very similar signals); and (d) pattern with $a = 250$ nm and $g = 160$ nm.

thickness varies between 20 and 40 nm. For the half-processed structure, consisting of a lifted-off membrane on top of a thick bottom metal layer, we also estimate $N = 12$. Therefore, in both structures, there is an equal increase in the pumping intensity resulting from the pump beam trapping in the microcavity.

IV. MEASUREMENTS

The experimental setup used for the PL measurements is shown in Fig. 17. Samples are mounted on an X-Y-Z stage and optically pumped at a 90° incident angle. The pump source is a semiconductor laser diode emitting at 830 nm, pulsed with a period of 3 μs and a pulse width of 2.5 μs. A nonpolarizing cube beamsplitter is used to bring 50% of the pump beam to the detector and to measure the external pump power. The other 50% of the beam is focused to a 10-μm spot on the sample by using a 100X objective lens (labeled as Lens 1). The same objective lens is also used to collect the emitted light. The collection angle is 30° with respect to normal. The collected emission is then focused in Lens 2 and detected using a fiber coupled spectrum analyzer.

We have measured the output from the unprocessed as-grown wafer, from the half-processed wafer, and from the fully processed structures, with a patterned or unpatterned thin metal layer on top. We fabricated a series of gratings in the top metal layer, that was 25 nm thick (within a ±10% range). Each grating is characterized with a periodicity (a) and a gap (g) between silver stripes. Between stripes, silver was completely removed by Ar$^+$ ion milling. During the thin silver layer deposition, part of the sample surface was masked, in order to also produce half-processed regions. The measurement results are summarized in Table II, where the peak external pump power was 2.2 mW. E_{up}(986 nm) and E_{hp}(986 nm) denote the PL enhancements at 986 nm of the fully processed wafer with respect to the unprocessed and half-processed wafers, respectively. Tabulated values are raw measured data and have not been rescaled. For all fully processed wafers, including the unpatterned metal clad microcavity, the FWHM is in the range of 60–110 nm. Therefore, their quality factors are between 10–15. For the half-processed wafer, the FWHM is 32 nm. Because of a bulk emission tail at lower wavelengths, a luminescence peak at 930 nm for unprocessed wafers cannot be clearly resolved. The spectra for unprocessed, half-processed and fully processed wafers are shown in Fig. 18. The PL peak of the unprocessed wafer at 986 nm was normalized to 1. A filter was applied before the detection to cut off wavelengths below 890 nm. A deposition of metal at one or at both sides of a 90-nm-thin semiconductor membrane does not seem to induce additional strain, since for all measured structures luminescence peaks are located at wavelengths of 986 and 930 nm.

In order to explain measurement results, we have to take into account several effects: A) the increase in the pumping intensity resulting from the trapping of pump photons within a microcavity; B) the decay rate enhancement; and C) the change in the external efficiency. In our explanation, we will use theoretical results presented in the previous section of this article. The spontaneous emission reabsorption is not very efficient because of the small optical confinement factor in the QW and the photon recycling effect can also be neglected [3].

If P_{in} denotes the external pump power and P_{out} denotes the power emitted from the device, then

$$\frac{P_{\text{out}}}{P_{\text{in}}} \cong \gamma \qquad (18)$$

where γ is defined as

$$\gamma = \beta \cdot (f_{\|} F_{d,\|} \eta_{\text{ext},\|} + f_{\perp} F_{d,\perp} \eta_{\text{ext},\perp}). \qquad (19)$$

For patterned structures, the first term should be separated into contributions of parallel dipoles in the x direction and in the z direction, since they have different η_{ext}. $f_{\|}$ and $f_{\perp}$ are fractions of dipole transitions that are in the QW plane or perpendicular to it. Their values at the main peak of 986 nm are $f_{\|} = 1$ and $f_{\perp} = 0$ and at 930 nm are $f_{\|} = 1/3$ and $f_{\perp} = 2/3$. Furthermore, $1/2$ of parallel dipoles are oriented in the x direction and the other half in the z direction. β is the equivalent pumping intensity that can be expressed as

$$\beta = T \cdot N. \qquad (20)$$

Let us label the half-processed wafer by a subscript hp, the unprocessed wafer using a subscript up, and denote the PL enhancement by E. If the input pump powers are the same (i.e., P_{in} equal), PL enhancements can be expressed as

$$E_{\text{hp}} = \frac{\gamma}{\gamma_{\text{hp}}} \qquad (21)$$

$$E_{\text{up}} = \frac{\gamma}{\gamma_{\text{up}}}. \qquad (22)$$

The half-processed wafer has a 21-fold PL intensity enhancement at 986 nm relative to the unprocessed wafer. This is a result of the increased external efficiency into the collection angle of $30°$ (by a factor of 2), the decay rate enhancement of $F_{d,\|} = 1.5$ and the higher pumping intensity resulting from pump photons trapping within the structure. Therefore, the pump trapping factor for the half-processed wafer is $N_{\text{hp}} = 7$.

The unpatterned metal clad microcavity has a sixfold PL intensity increase at 986 nm and the prominent peak at 930 nm. Relative to the half-processed wafer, PL enhancements at 986 and 930 nm are equal to 0.26 and 1.5, respectively. In order to explain this result, we calculated $(\gamma N_{\text{hp}}/\gamma_{\text{hp}} N)$. The result is shown in in Fig. 19. Parameters without a subscript refer to the unpatterned metal clad microcavity. We theoretically predicted that $N \cong N_{\text{hp}}$. For the top silver layer thickness of 27 nm, the theoretically estimated E_{hp} values agree with the experimentally observed ones. For this silver layer thickness, we have estimated theoretically $F_{d,\|}(986\,\text{nm}) = 0.5$, $F_{d,\|}(930\,\text{nm}) = 2.1$, $\eta_{\text{ext},\|}(986\,\text{nm}) = 6\%$ and $\eta_{\text{ext},\|}(930\,\text{nm}) = 12\%$ (into the $30°$ collection angle). Therefore, the increase in the PL intensity has to be a result of an increase in the efficiency, defined as $F_d \cdot \eta_{\text{ext}}$, which is six times larger than in the unprocessed wafer at 986 nm. Furthermore, the enhancement in the 930-nm peak comes from the Purcell enhancement and the improved extraction for parallel dipoles.

Is it possible that the enhanced peak at 930 nm is a result of the unpatterned structure pumped stronger than the half-processed one? Since the transmission coefficient T of the unpatterned structure is at least ten times smaller than the one of the
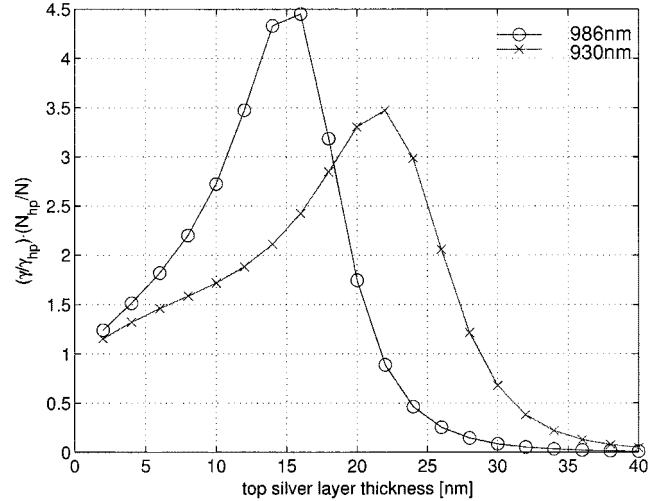

Fig. 19. Ratio of γ factors for the unpatterned metal clad microcavity and the half-processed structure.

half-processed structure for the top silver layer thickness larger than 25 nm, the stronger pumping of the unpatterned structure would require $N/N_{\text{hp}} > 10$. However, according to Fig. 19 and for the experimentally observed PL enhancement at 986 nm, this would imply that $(\gamma N_{\text{hp}}/\gamma_{\text{hp}} N) < 0.025$, which is possible only for thicker silver layers (thicker than 35 nm). This not the case in our structure and, therefore, the enhanced peak at 930 nm cannot be a result of the strong pumping. In order to prove experimentally that the enhancement of the peak at 930 nm is not a result of the strong pumping, we measured the PL of the unpatterned microcavity at different pumping levels. The external pump power was controlled by neutral density filters. The shape of the PL spectra did not change when the pumping level was reduced.

Structures with periodicities of 480 or 650 nm have a similar performance to the unpatterned metal clad microcavity, as we theoretically predicted.

The structure with a periodicity of 250 nm has a 46-fold PL intensity enhancement at 986 nm relative to the unprocessed wafer. Clearly, we cannot determine exactly T and N factors for the patterned structure, but we can make a rough estimate and confirm that there is definitely an increase in the efficiency relative to the unprocessed wafer. Let us assume that the N factor is of the same order as that of the half-processed wafer, and use the theoretically estimated value of the transmission coefficient $(T = 40\%)$. Then, we estimate that the pumping intensity has increased 4 times relative to the unprocessed wafer. This means that there is a 12-fold increase in the efficiency (into the detection angle of $30°$) compared to the unprocessed wafer. The PL peak at 930 nm is not as large as in the unpatterned top layer case. The weaker peak at 930 nm can be explained by the fact that the Purcell enhancement at 930 nm is not as strong as in the unpatterned structure.

V. CONCLUSION

We have theoretically analyzed, fabricated, and measured the metal clad microcavity with a sub-$\lambda/2$ semiconductor membrane and a patterned top metal layer. The emitting region is

a single QW positioned in the middle of the membrane. At the same external pump power, we measure PL enhancements of up to 46 times with respect to the unprocessed wafer. We estimate that this enhancement is due to at least a 12-fold increase in the efficiency (relative to an unprocessed wafer), and an increase in the effective pumping intensity resulting from the pump photons trapping within the microcavity. Interesting modifications in the PL spectra were also experimentally observed, resulting from the simultaneous change in the spontaneous emission rate and the extraction efficiency.

Therefore, we showed that the coupling to surface plasmons in the patterned metal clad microcavity can be used to improve the light extraction and enhance the spontaneous emission rate in light-emitting devices. One of the advantages of this design is the small surface recombination rate, since the semiconductor is not perforated. Furthermore, metallic layers that are already included in the design can also be used as contacts for electrical pumping of the device. Certainly, in order to make good contacts, more attention has to be paid to the proper choice of metal. Devices presently operate in the 980-nm wavelength range, where metal absorption losses are significant. This reduces quality factors of fully processed structures to values between 10–15 and broadens their emission. This problem can be overcome by designing devices that operate at longer wavelengths. For example, a surface plasmon laser operating at 17 μm has been demonstrated recently by researchers in Bell Labs [23].

We conclude that metal clad microcavities can be used as building blocks for highly efficient LEDs. However, in order to make a practical device, more research and work has to be done, particularly in designing their electrical properties.

Acknowledgment

References

[1] I. Schnitzer, E. Yablonovitch, C. Caneau, T. J. Gmitter, and A. Scherer, "30% external quantum efficiency from surface textured, thin film light-emitting diodes," *Appl. Phys. Lett.*, vol. 63, no. 16, pp. 2174–2176, Oct. 1993.

[2] E. F. Schubert, N. E. J. Hunt, M. Micovic, R. J. Malik, D. L. Sivco, A. Y. Cho, and G. J. Zydzik, "Highly efficient light-emitting diodes with microcavities," *Science*, vol. 265, pp. 943–945, Aug. 1994.

[3] T. Baba, R. Watanabe, K. Asano, F. Koyama, and K. Iga, "Theoretical and experimental estimations of photon recycling effect in light emitting devices with a metal mirror," *Jpn. J. Appl. Phys.*, vol. 35, pp. 97–100, Jan. 1996.

[4] A. Kock, E. Gornik, M. Hauser, and W. Beinstingl, "Strongly directional emission from AlGaAs/GaAs light-emitting diodes," *Appl. Phys. Lett.*, vol. 57, no. 22, pp. 2327–2329, 1990.

[5] R. Windisch, P. Heremans, A. Knobloch, P. Kiesel, G. H. Dohler, B. Dutta, and G. Borghs, "Light-emitting diodes with 31% external quantum efficiency by outcoupling of lateral waveguide modes," *Appl. Phys. Lett.*, vol. 74, no. 16, pp. 2256–2258, Apr. 1999.

[6] E. M. Purcell, "Spontaneous emission probabilities at radio frequencies," *Phys. Rev.*, vol. 69, pp. 681–681, 1946.

[7] J. Gerard, B. Sermage, B. Gayral, B. Legrand, E. Costard, and V. Tierry-Mieg, "Enhanced spontaneous emission by quantum boxes in a monolitic optical microcavity," *Phys. Rev. Lett.*, vol. 91, no. 5, pp. 1110–1113, 1998.

[8] I. Gontijo, M. Boroditsky, E. Yablonovitch, S. Keller, U. K. Mishra, and S. P. DenBaars, "Coupling of InGaN quantum-well photoluminescence to silver surface plasmons," *Phys. Rev. B*, vol. 60, no. 16, pp. 11 564–11 567, Oct. 1999.

[9] M. Boroditsky, R. Vrijen, T. F. Krauss, R. Coccioli, R. Bhat, and E. Yablonovitch, "Spontaneous emission extraction and purcell enhancement from thin-film 2-D photonic crystals," *J. Lightwave Technol.*, vol. 17, pp. 2096–2112, Nov. 1999.

[10] W. L. Barnes, "Electromagnetic crystals for surface plasmon polaritons and the extraction of light from emissive devices," *J. Lightwave Technol.*, vol. 17, pp. 2170–2182, Nov. 1999.

[11] L. A. Coldren and S. W. Corzine, *Diode Lasers and Photonic Integrated Circuits*. New York: Wiley, 1995.

[12] E. Yablonovitch, D. M. Hwang, T. J. Gmitter, L. T. Florez, and J. P. Harbison, "Van der Waals bonding of GaAs epitaxial liftoff films onto arbitrary substrates," *Appl. Phys. Lett.*, vol. 56, no. 24, pp. 2419–2421, June 1990.

[13] S. A. Cummer, "An analysis of new and existing FDTD methods for isotropic cold plasma and a method for improving their accuracy," *IEEE Trans. Antennas Propagat.*, vol. 45, pp. 392–400, Mar. 1997.

[14] J. B. Judkins and R. W. Ziolkowski, "Finite-difference time-domain modeling of nonperfectly conducting metallic thin-film gratings," *J. Opt. Soc. Amer. B*, vol. 12, no. 9, pp. 1974–1983, 1995.

[15] K. S. Yee, "Numerical solution to initial boundary value problems involving Maxwell's equations in isotropic media," *IEEE Trans. Antennas Propagat.*, vol. AP-14, pp. 302–307, May 1966.

[16] A. Taflove, *Computational Electrodynamics—The Finite-Difference Time-Domain Method*. Norwood, MA: Artech House, 1995.

[17] O. Painter, J. Vučković, and A. Scherer, "Defect modes of a two-dimensional photonic crystal in an optically thin dielectric slab," *J. Opt. Soc. Amer. B*, vol. 16, no. 2, pp. 275–285, Feb. 1999.

[18] G. Mur, "Absorbing boundary conditions for the finite-difference approximation of the time-domain electromagnetic-field equations," *IEEE Trans. Electromagn. Compat.*, vol. EMC-23, pp. 377–382, Nov. 1981.

[19] S. C. Kitson, W. L. Barnes, and J. R. Sambles, "Photonic band gaps in metallic microcavities," *J. Appl. Phys.*, vol. 84, no. 5, pp. 2399–2403, 1998.

[20] J. A. E. Wasey and W. L. Barnes, "Efficiency of spontaneous emission from planar microcavities," *J. Mod. Opt.*, vol. 47, no. 4, pp. 725–741, 2000.

[21] M. S. Tomaš and Z. Lenac, "Damping of a dipole in planar microcavities," *Opt. Commun.*, vol. 100, no. 1–4, pp. 259–267, 1993.

[22] Y. Xu, J. S. Vučković, R. K. Lee, O. J. Painter, A. Scherer, and A. Yariv, "Finite-difference time-domain calculation of spontaneous emission lifetime in a microcavity," *J. Opt. Soc. Amer. B*, vol. 16, no. 3, pp. 465–474, 1999.

[23] A. Tredicucci, C. Gmachl, F. Capasso, and A. L. Hutchinson, "Single-mode surface-plasmon laser," *Appl. Phys. Lett.*, vol. 76, no. 16, pp. 2164–2166, 2000.

Jelena Vučković was born in Niš, Yugoslavia, in 1971. She received the Dipl.Ing. degree from the Faculty of Electronic Engineering, University of Niš, Yugoslavia, in 1993. In 1997, she received the M.S. degree in electrical engineering from the California Institute of Technology, Pasadena, where she is currently working toward the Ph.D. degree.

From 1994 to 1995, she was with the University of Niš as an Assistant, and during 1996, she was with the School of Electrical Engineering, University of Sydney, Australia, as a Researcher. Her research interests include the design and fabrication of optical microcavities and photonic crystal-based optical devices.

Marko Lončar was born in Dubrovnik, Croatia, in 1974. He has received the Dipl.Ing. degree from the Faculty of Electrical Engineering, University of Belgrade, Yugoslavia, in 1997, and the M.S. degree in electrical engineering from the California Institute of Technology, Pasadena, in 1998. Currently, he is working toward the Ph.D. degree in electrical engineering at the California Institute of Technology.

His research interests include design and fabrication of photonic crystal devices and ultrasmall device processing techniques.

Axel Scherer received the B.S., M.S., and Ph.D. degrees from the New Mexico Institute of Mining and Technology,Socorro, in 1981, 1982, and 1985, respectively.

From 1985 until 1993, he worked in the Quantum Device Fabrication group at Bellcore. Currently he is Professor of Electrical Engineering, Applied Physics, and Physics at the California Institute of Technology, Pasadena, specializing in device microfabrication. His research interests include design and fabrication of functional photonic, nanomagnetic, and microfluidic devices.